Heliyon

Received:
27 June 2018
Revised:
27 November 2018
Accepted:
17 December 2018

Cite as: Takayuki Odahara, Koji Odahara. Various salts employed as precipitant in combination with polyethylene glycol in protein/detergent particle association. Heliyon 4 (2018) e01073.
doi: 10.1016/j.heliyon.2018.e01073

Various salts employed as precipitant in combination with polyethylene glycol in protein/detergent particle association

Takayuki Odahara [a,*], **Koji Odahara** [b]

[a] *National Institute of Advanced Industrial Science and Technology (AIST), Tsukuba Central−6, 1−1 Higashi, Tsukuba, Ibaraki, 305−8566 Japan*

[b] *Fukuoka Prefectural Association of Agricultural Production and Materials, Fukuoka Prefectural Office, Hakata, Fukuoka, 812−8577 Japan*

[*] Corresponding author.
E-mail address: odahara-takayuki@aist.go.jp (T. Odahara).

Abstract

Salt/polyethylene glycol (PEG) mixtures are employed as precipitants for biological macromolecules. The dependence of precipitation curves (PCs) on salt species was investigated for integral membrane protein/detergent particles. By relating this dependence to properties of ions dissociated from added salts, the following roles and effects of various ions were clarified. In the presence of ions whose interaction with water is stronger than water−water interaction, the coordination of solvent molecules is rearranged so as to strengthen short-range steric repulsion and hydrophobic attraction. Ions whose interaction with water is weaker than water−water interaction can be a hindrance to hydrophobic−hydrophobic contact. Moreover, strong electric fields of divalent cations can cause an attractive effect between electronegative or polar groups of neighboring particles. The variations of particle−particle and particle−PEG interactions depending on the state of particles and surrounding solvents were correlative. Due to this, the relationship between the horizontal positions of PC and the species of salts

https://doi.org/10.1016/j.heliyon.2018.e01073

added could be formulated as a binary linear function of cationic and anionic species composing the salts.

Keywords: Biochemistry, Physical chemistry, Inorganic chemistry

1. Introduction

Polyethylene glycol (PEG) has a relatively mild influence on the structures of macromolecules. Thus, mixtures of PEG and various salts are widely used as precipitants to fractionate [1, 2, 3], concentrate, and crystallize [4, 5, 6] biological macromolecules such as proteins. With respect to macromolecular crystallization, although high-throughput techniques to search suitable solution compositions have been rapidly advanced with development of robotics and computer science [7], the mechanism remains unclear. To elucidate the mechanism, the roles and effects of salts and PEG in macromolecular association (including crystallization) need to be clarified.

The analysis of chemical potentials of components in a ternary system shows that macromolecule−macromolecule interaction in the absence of PEG and macromolecule−PEG interaction are reflected by values of intercept and slope of precipitation curves (PCs), respectively [3]. Moreover, the dependence of PCs on salt concentration shows that the variations of the two kinds of interactions by addition of salts can be interpreted in terms of solvent effects such as short-range steric repulsions, ion-correlation force, ionic bridging and hydrophobic attractions in addition to electrostatic forces [8]. On the other hand, the studies of crystal growth based on phase diagrams show that PEG concentrations adequate for crystallization of macromolecules are evaluated by referring to the PCs [6, 9]. Regarding effects of various salts employed as precipitants in combination with PEG, however, it is still unknown whether a relationship exists such as a 'lyotropic series' [10, 11] in the absence of PEG. Even for the same macromolecule, appropriate PEG concentrations should be established for every salt species by trial-and-error.

Our objective in this study is to advance understanding of the effectiveness of various salts in macromolecular association and to obtain relationships for practical use. Towards this objective, the dependence of PC on salt species was investigated for various protein/detergent particles with different physicochemical properties. The roles and effects of individual ions dissociated from the added salts in the particle association were clarified by relating the observed dependence of PC to the properties of ions. Moreover, the observed relationships between horizontal positions of PC and ionic species were formulated by using a set of values reflecting the density and distribution of electric charges in ions.

https://doi.org/10.1016/j.heliyon.2018.e01073

2. Materials and methods

2.1. Preparation of protein/detergent particles and their properties

Rhodobacter (*Rb.*) *capsulatus* light-harvesting protein−pigment complex 2 (LH2), *Rb. sphaeroides* LH2 and photoreaction center (RC), *Rhodopseudomonas* (*Rp.*) *viridis* RC and RC with light-harvesting protein−pigment complex 1 (PRU) were purified according to published methods [8, 9, 12, 13, 14, 15, 16, 17]. The final protein solutions were prepared according to reported methods [8, 9].

The properties of these proteins were evaluated in our previous study [8]. Briefly, the molecular weight increases in the order *Rb. sphaeroides* RC (94000) < *Rb. capsulatus* LH2 (95000) < *Rb. sphaeroides* LH2 (99000) < *Rp. viridis* RC (132000) < *Rp. viridis* PRU (339000). On the other hand, the Stokes radii of these proteins solubilized by *N*−dodecyl−β−*D*−maltopyranoside (LM) increase in the following order; *Rb. sphaeroides* RC (4.4 nm) < *Rp. viridis* RC (5.0 nm) < *Rb. sphaeroides* LH2 (6.1 nm) < *Rb. capsulatus* LH2 (6.2 nm) < *Rp. viridis* PRU (6.4 nm). The isoelectric points (pIs) determined by isoelectric focusing are 3.5−3.8 for *Rb. capsulatus* LH2/LM, 3.5−4.2 for *Rb. sphaeroides* LH2/LM, 4.0−4.5 for *Rb. sphaeroides* RC/LM, 7.1−8.0 for *Rp viridis* RC/LM and 7.4−8.1 for *Rp viridis* PRU/LM. The ratio of surface area of detergent cluster to that of particle increases in the order; *Rp. viridis* PRU (55%) < *Rp. viridis* RC (65%) < *Rb. sphaeroides* RC (70%) < *Rb. capsulatus* LH2 = *Rb. sphaeroides* LH2 (85%).

2.2. Determination of precipitation curves based on protein concentrations in supernatant

Highly concentrated solutions of protein (50 mg/mL), salt (1−8 M), PEG 4000 (625 mg/mL), buffer (0.5 M), and detergent (200 mg/mL) were put into a small test tube (0.5 mL), and were vigorously mixed on a vortex mixer. The total protein concentration was adjusted to be 20 mg/mL in all the final sample solutions of 0.05 mL. For efficient pipetting of viscous sample solution, micromans (GILSON) were used. After amorphous precipitates of the protein/detergent particles were removed from the mixed solutions by centrifugation at 12,000 rpm (Hitachi T15AP21) for 6 min, the protein concentration in the supernatant was photometrically evaluated using the absorption coefficient characteristics to each relevant protein. Those operations were performed at 21−23 °C. It was difficult to determine precise concentrations of protein/detergent particles due to the adhering nature of detergents, but the particle concentrations were thought to reflect concentrations of relevant proteins proportionally. Hence, we employed the protein concentration instead of the concentration of protein/detergent particles. The concentrations of *Rb. capsulatus* LH2, *Rb. sphaeroides* LH2 and RC, and *Rp. viridis* RC and PRU were based on the relationship that one

https://doi.org/10.1016/j.heliyon.2018.e01073

absorbance unit at 800, 800, 800, 830, and 1020 nm corresponds to 0.083, 0.083, 0.33, 0.45, and 0.086 mg protein/mL, respectively [9].

For each salt species, the protein concentrations $[D]_{ppt}$ in the supernatant were mostly correlated to PEG concentrations [P] by the following Eq. (1) [1, 6, 8, 9]:

$$[D]_{ppt} = A_{ppt}\exp\left(-B_{ppt}[P]\right), \quad (1)$$

where A_{ppt} and B_{ppt} are constants specific to individual protein/detergent particles.

PCs were obtained by least-square fittings of this equation to the experimental values [6, 8, 9]. To confirm reproducibility of the results for proteins in the native states, the PCs were drawn on the basis of supernatant protein concentration measured within 30 min after the addition of salt/PEG mixtures [7, 9, 18]. To precisely compare the effects of each salt species, the same solutions of the proteins and chemicals were employed in each series of experiments.

3. Results and discussion

3.1. Salt concentrations employed in determining precipitation curves

In our previous study [8], the dependence of PC on salt concentrations was investigated for five kinds of proteins. From the dependence, an 'effective concentration' was deduced so that various salt species could exert the electrostatic screening effect to the same extent. The 'effective concentration' $[S]_{eff}$ of a salt S was defined as a product of molarity [S] of the salt and a coefficient α that was 1, 2, 3, 10, and 10 for 1:1 salts such as KNO_3, 1:2 salts such as $K_2(SO_4)_2$, 1:3 salts such as tri-potassium citrate, 2:1 salts such as $Mg(NO_3)_2$, and 2:2 salts such as $MgSO_4$, respectively.

Upon increasing the PEG and/or salt, a stage comes at which salt- and PEG-rich aqueous phases become immiscible with each other and separate [8, 18, 19, 20, 21]. When the 'effective concentrations' of K_2HPO_4 and tri-potassium citrate were 0.5 or higher, the influence of salt−PEG mutual separation brought about a steep increase in the intercept and slope values of the PC of *Rb. sphaeroides* LH2 solubilized by *N*−octyl−β−*D*−glucoside (OG). However, we made sure that the variation of PC with salt concentration reached a plateau at 0.4 in terms of the 'effective concentration' unit. Moreover, the PCs of *Rp. viridis* PRU and RC, *Rb. sphaeroides* RC and LH2 and *Rb. capsulatus* LH2 solubilized by LM exhibited no variation at salt concentrations above 0.2, 0.15, 0.16, 0.4 and 0.3 in terms of the 'effective concentration' unit, respectively. Thus, at the 'effective concentration' of 0.4, the PCs were not much influenced by the mutual separation of salt and PEG, and then the concentration-dependent influence of salt on the PC reached a plateau.

https://doi.org/10.1016/j.heliyon.2018.e01073

From these results, it was expected that PCs at an 'effective concentration' of 0.4 would reveal salt species-dependent effects on particle−particle and particle−PEG interactions that were common to the five kinds of proteins. On this account, the salt concentrations corresponding to 0.4 in terms of the 'effective concentration' unit were employed throughout this study. Additionally, at these salt concentrations, the five kinds of proteins are in a state where the electrostatic fields surrounding the protein/detergent particles are sufficiently screened [8].

3.2. PC of *Rb. shaeroides* LH2/OG for various kinds of nitrates and potassium salts

3.2.1. Variation in solvent effects by addition of salt

Many kinds of salts are dissociated into ions in an aqueous solution with high dielectric constant. The dissociated ions are different from water molecules in properties such as electric charge, dipole moment, size and shape. Therefore, when ions displace some water molecules previously existing around the macromolecules, not only macromolecule−macromolecule interactions but also macromolecule−solvent and solvent−solvent interactions are altered, as explained below.

Magnitude and range of direct electrostatic forces between macromolecules are reduced due to the electrostatic screening effect of ions. Hence, macromolecules can mutually approach without their electrostatic interactions to such a level where the first or second shells of solvent molecules such as water molecules and ions around them begin to mutually overlap [8, 11]. Moreover, when ions attractively interact with hydrophilic groups of one macromolecule, the ions hinder the groups getting in contact with not only hydrophilic groups but also hydrophobic groups of the other macromolecule. The steric repulsion based on the attracted ions, due to the short-range nature, has an effect to disperse macromolecules in aqueous solutions. When the electric field of ion itself becomes stronger, the ions are more strongly attracted to the macromolecular surface, and hence macromolecules can be more stably dispersed. Additionally, affinity of hydrophilic groups to the aqueous phase becomes higher by mediation of ions with a strong electric field on their surfaces, since the ions also strongly interact with water molecules as well as hydrophilic groups. The total effect caused by ions attracted to hydrophilic groups will be referred to as hydrophilic 'repulsion' hereafter.

On the other hand, ions with a strong electric field not only disorganize networks of hydrogen-bonding water molecules but also tend to move into the bulk solution to interact with as many water molecules as possible. These two effects of ions, coupled with the effect to strengthen surface tension of aqueous solvent [11, 22], prompt contact of hydrophobic groups. Thus, the tendency of hydrophobic contact between macromolecules is more strengthened by the presence of ions with stronger electric

https://doi.org/10.1016/j.heliyon.2018.e01073

fields. Although the effect to prompt hydrophobic contact is not based on a real force, we will refer to it as hydrophobic 'attraction' hereafter. Thus, when macromolecules mutually approach within a short distance, a few times the diameters of a solvent molecule, the intermacromolecular interaction is determined by the compromise between the short-range steric repulsion and the hydrophobic 'attraction' that have opposing effects on the macromolecular association.

3.2.2. Influence of different monovalent cations on the interaction between Rb. shaeroides LH2/OG particles

Fig. 1 shows the PCs of *Rb. shaeroides* LH2 solubilized by OG (*Rb. shaeroides* LH2/OG) in Tris buffer (25 mM Tris−HCl, and 0.2 mg/mL NaN_3; pH 8.0) to which various salts were added separately. Since the plot of *ln* $[D]_{ppt}$ versus [P] exhibited a good linear relationship with a correlation coefficient of $\geq$0.99, the standard errors of A_{ppt} were similar to or smaller than the size of symbols in the figure. Besides, the standard errors shown in Table 1 were evaluated from ten PCs determined for each of the three different *Rb. shaeroides* LH2 particles by the use of the same sample solution; they were standard errors depending on timing of experiment. Even if the influences of these standard errors were taken into consideration, the A_{ppt} values were smaller than the values ($> 10^{14}$ mg protein/mL) in the absence of a salt that were evaluated from the dependence of A_{ppt} on salt concentration [8]. This result suggests that the addition of salts strengthens hydrophobic 'attraction' more than hydrophilic 'repulsion' between the particles. This agrees with the property of *Rb. sphaeroides* LH2 that consists of several moieties composed of 4 or more consecutive hydrophobic residues in the extra-micellar regions [8, 23, 24].

The interaction between a nitric ion and a water molecule is very weak, as understood from the hydration number of the ion [25]. It follows that neither the state of water molecules interacting with hydrophilic groups nor the state of hydrogen-bonding water molecules around hydrophobic groups is significantly disorganized in the presence of nitric ions. This suggests that the variation of A_{ppt} for nitrates with different cations largely reflects the change in the particle−particle interaction depending on the cationic species.

For nitrates, even if the influences of standard errors mentioned above were taken into consideration, the value of A_{ppt} increased in the following order along the ascending $[D]_{ppt}$: Cd^{2+} (9.1×10^2 mg/mL) < Ni^{2+} (3.6×10^3 mg/mL) < Zn^{2+} (8.6×10^3 mg/mL) < Mn^{2+} (1.9×10^4 mg/mL) $\leq$ Co^{2+} (2.3×10^4 mg/mL) < Ca^{2+} (7.2×10^4 mg/mL) < Mg^{2+} (1.5×10^5 mg/mL) < NH_4^+ (2.6×10^5 mg/mL) < K^+ (3.4×10^5 mg/mL) $\leq$ Na^+ (3.8×10^5 mg/mL) $\leq$ Li^+ (4.1×10^5 mg/mL) (Fig. 1A). The value of A_{ppt} provides a measure of the threshold particle−particle separation above which the particles can behave independently of one another while their being still dispersed in the solution. The magnitude and

https://doi.org/10.1016/j.heliyon.2018.e01073

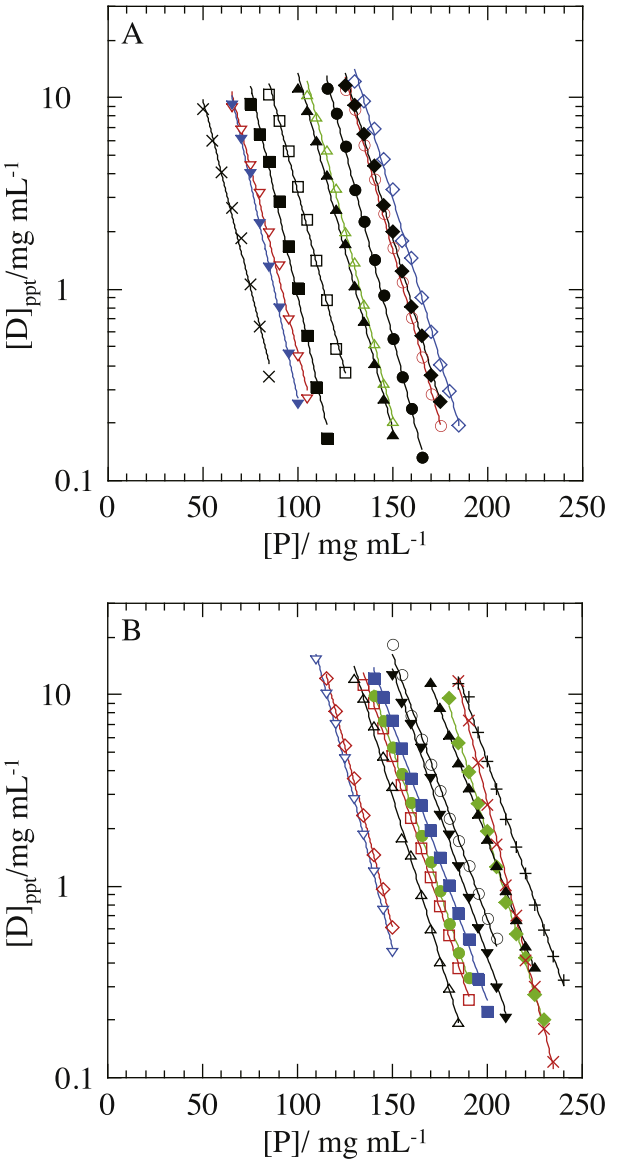

Fig. 1. Precipitation curves (PCs) of *Rb. sphaeroides* LH2 solubilized by OG against polyethylene glycol (PEG) concentration for various salt species. The PCs were obtained by least-square fitting of Eq. (1) to the supernatant protein concentrations $[D]_{ppt}$ against PEG concentration [P]. A; the added nitrates and their concentrations were 0.4 M $LiNO_3$ (◯), 0.4 M $NaNO_3$ (●), 0.4 M KNO_3 (◇), 0.4 M NH_4NO_3 (◆), 0.04 M $Mg(NO_3)_2$ (△), 0.04 M $Ca(NO_3)_2$ (▲), 0.04 M $Mn(NO_3)_2$ (□), 0.04 M $Co(NO_3)_2$ (■), 0.04 M $Ni(NO_3)_2$ (▽), 0.04 M $Zn(NO_3)_2$ (▼), and 0.04 M $Cd(NO_3)_2$ (×). B; the added potassium salts and their concentrations were 0.4 M KF (◯), 0.4 M KCl (□), 0.4 M KI (◇), 0.4 M KNO_3 (△), 0.4 M KSCN (▽), 0.4 M potassium formate (●), 0.4 M potassium acetate (■), 0.2 M K_2SO_4 (◆), 0.2 M potassium oxalate (▲), 0.2 M potassium tartrate (▼), 0.2 M K_2HPO_4 (×), and 0.133 M potassium citrate (+). The other solution ingredients were 25 mM Tris−HCl (pH 8.0), 0.2 mg/mL NaN_3, and 8 mg/mL OG.

https://doi.org/10.1016/j.heliyon.2018.e01073

Table 1. Relative standard errors of PC of *Rb. sphaeroides* LH2 particles depending on timing of experiments.

	Rb. sphaeroides **LH2/LDAO**	***Rb. sphaeroides*** **LH2/OG**	***Rb. sphaeroides*** **LH2/LM**
A_{ppt} Mean value/mg mL^{-1}	1650000	340000	75800
Standard error/mg mL^{-1}	354000	35700	14400
Relative standard error/%	22	11	19
B_{ppt} Mean value	0.0743	0.0747	0.0957
Standard error	0.0011	0.0008	0.0017
Relative standard error/%	1.5	1.1	1.8
$[P]_5$ Mean value/mg mL^{-1}	171	149	100
Standard error/mg mL^{-1}	0.19	0.41	0.21
Relative standard error/%	0.11	0.28	0.21

range of electrostatic force directly acting between the particles was sufficiently reduced at the salt concentrations employed. Moreover, it is thought that van der Waals dispersion force is not much affected by electrostatic screening effects of ions [26]. For these reasons, it is hardly conceivable that those electric forces would vary significantly further depending on the salt species added. Therefore, the different values of A_{ppt} for the cations are not ascribable to the difference in the magnitude of electric forces already screened.

The maximum interaction energies [25] calculated for Li^+, Na^+ and K^+ adjacent to a water molecule are 2.1×10^{-19} J, 1.6×10^{-19} J and 1.2×10^{-19} J, respectively. The ammonium ion possesses large dipole moments along the N−H bonds in addition to a positive charge of electron-depleted proton bound to the ion. From these, it is understood that the ion−water interaction energies are comparable to or greater than the interaction energy 1.3×10^{-19} J between two water molecules whose dipoles are lying in line. Therefore, networks of hydrogen-bonding water molecules, which mask hydrophobic groups on the particle surface, are disrupted in the presence of these monovalent cations. As a result, at the comparatively high salt concentrations employed, the hydrophobic groups can be fully exposed to the aqueous phase. On the other hand, affinity of hydrophilic groups to the aqueous phase becomes higher with strengthening electric field of ions themselves, that is, in the order $NH_4^+ < K^+ < Na^+ < Li^+$ [8]. Thus, although the addition of a salt strengthens hydrophobic 'attraction' more than short-range steric repulsion between the particles, the dependence of A_{ppt} on monovalent cations exhibits a variation characteristic of short-range steric repulsion.

https://doi.org/10.1016/j.heliyon.2018.e01073

3.2.3. Influences of different divalent cations on the interaction between Rb. shaeroides LH2/OG particles

The values of A_{ppt} for divalent cations were smaller than those for monovalent cations, though the salt concentrations in the case of divalent cations were lower than those in the case of monovalent cations by a factor of ten in molarity. Moreover, the amorphous precipitates formed in the presence of divalent cations were more rigid than those in the presence of monovalent cations. These results suggest that the particle−particle attractive interaction in the presence of divalent cations is stronger than the hydrophobic 'attraction' in the presence of monovalent cations. Mobile divalent cations in electrical double-layers and negative charges on the particle surfaces constitute large dipole moments that can cause a strong attractive effect such as ion-correlation force [27, 28, 29] between the neighboring particles. Besides, when a divalent cation exists between electronegative groups on the surfaces of two neighboring particles, due to its strong electric field, it can form an ionic bridge between the particles. Thus, some of the divalent cations adjacent to the particle surfaces can induce these strong effects instead of short-range steric repulsion. This seems to be the reason for the smaller values of A_{ppt} for divalent cations than for monovalent cations.

In the presence of divalent cations, the particle−particle interaction is expected to be strengthened in the order $Ca^{2+} < Mg^{2+} < Cd^{2+} < Zn^{2+} < Mn^{2+} < Co^{2+} < Ni^{2+}$, because the electric field of divalent cations themselves is thought to strengthen in the same order [8]. However, this order of ions along the strengthening electric field disagrees with that along the descending A_{ppt}. This disagreement seems to be due to that the stronger the electric field of ions themselves, the more the electrostatic energy of ions is expended for binding water molecules and aligning them around the ions.

3.2.4. Influences of different anions on the interaction between Rb. shaeroides LH2/OG particles

For potassium salts comprised of different anions, even if the influences of the two kinds of standard errors were taken into consideration, the A_{ppt} increased in the following order: acetic$^-$ (1.6×10^5 mg/mL) $\leq$ formic$^-$ (1.7×10^5 mg/mL) = Cl^- (1.7×10^5 mg/mL) < F^- (2.2×10^5 mg/mL) $\leq$ SCN^- (2.5×10^5 mg/mL) = I^- (2.6×10^5 mg/mL) < NO_3^- (3.4×10^5 mg/mL) < tartric^{2-} (4.3×10^5 mg/mL) < oxalic^{2-} (4.8×10^5 mg/mL) << citric^{3-} (3.2×10^6 mg/mL) < SO_4^{2-} (8.5×10^6 mg/mL) << HPO_4^{2-} (2.5×10^8 mg/mL) (Fig. 1B). One feature of this order is that the larger the anionic charge number, the larger the value of A_{ppt}, which is opposite to the dependence of A_{ppt} on cationic charge number. The dependence on the anionic charge number is exemplified by the variation of A_{ppt} for carboxylic ions in which the number of carboxyl groups is not the same. The interaction

https://doi.org/10.1016/j.heliyon.2018.e01073

strength of carboxylic ions with hydrophilic groups does not vary depending on the ionic charge number to a large extent, because each negative charge (that is, each electron) of the carboxylic ions is found on each carboxyl group. However, multivalent carboxylic ions can simultaneously interact with hydrophilic groups on the particle surface and water molecules in the solution phase. In addition, the range of short-range steric repulsion between the particles is enlarged with an increase in the charge number, because the ionic size increases with an increase in the number of carboxyl groups. On the other hand, it is unlikely that the interparticle hydrophobic 'attraction' differs for the carboxylic ions more than the interparticle steric repulsion, because of the following reason. Networks of water molecules around hydrophobic groups are significantly disorganized in the presence of potassium ion, as explained above. Moreover, the strength and number of interactions between the ions and water molecules are comparable in all cases examined, because the carboxylates are separately added to the solution so that the number of water molecules to interact with the carboxyl groups can be the same. Thus, carboxylic ions with a larger charge number more hinder the particle−particle contact, whereas hydrophobic 'attraction' does not much vary depending on the ionic species.

Carboxylic ions, NO_3^-, SO_4^{2-} and HPO_4^{2-} have electronegative oxygen atoms that can attractively interact with electropositive groups, polar groups and water molecules. From the number of electrons attracted by the anions and the number of equivalent oxygen atoms in the resonance structures, it is roughly evaluated that the probability of finding one of the attracted electrons on each oxygen atom increases in the order NO_3^- (1/3) < -COO^- (1/2) = SO_4^{2-} (1/2) < HPO_4^{2-} (2/3). Moreover, the difference between electronegativities of atoms participating in the covalent bonds in the ions increases in the order N−O (0.40) < S−O (0.86) ≤ C−O (0.89) < P−O (1.25). These deduced orders agree with the order of divalent anions along the ascending A_{ppt}: tartric^{2-} < oxalic^{2-} << SO_4^{2-} << HPO_4^{2-}. Thus, it should be well comprehended that the effect of ions to hinder the particle−particle contact strengthens with increasing partial charge density of each oxygen atom.

However, if it is considered that a carboxyl group and a sulfate ion in fully ionized states are similar to each other in the two electrical properties mentioned in the preceding paragraph, the values of A_{ppt} for tartric^{2-} and oxalic^{2-} are too small in comparison with the value of A_{ppt} for SO_4^{2-}. The configuration of electronegative oxygen atoms in the carboxylic ions is asymmetrical, unlike that in SO_4^{2-}. Due to this difference, the strength of interaction between a carboxylic ion and a hydrophilic group varies more greatly depending on the angle at which they are oriented relative to each other than that of SO_4^{2-}. As a result, the number of carboxylic ions that strongly interact with charges and dipoles on the particle surface is smaller than that of SO_4^{2-}. This seems to be reflected as the smaller values of A_{ppt} for the carboxylic ions.

https://doi.org/10.1016/j.heliyon.2018.e01073

For halide ions, the value of A_{ppt} tended to decrease with increasing ionic charge density. This tendency is opposite to the relationship between the values of A_{ppt} and the charge density of monovalent cations. The maximum interaction energies calculated for halide ions adjacent to a water molecule suggest that the ion−water interaction is not so strong as the water−water interaction and weakens in the order $(H_2O) > F^- > Cl^- > I^-$. This relationship also agrees with the hydration number of halide ions [25]. Due to such a weak interaction, halide ions cannot fully disrupt networks of water molecules. However, they can approach hydrophobic groups around which networks of water molecules are disorganized in the presence of potassium ion. The number of halide ions staying around the hydrophobic groups increases in the order $F^- < Cl^- < I^-$. This is because the tendency of halide ions to be surrounded by water molecules, that is, their tendency to move into bulk solution, weakens in the same order.

Moreover, the A_{ppt} exhibited similar values for thiocyanic ion, iodic ion and nitric ion to which water molecules are not constantly bound [25]. The A_{ppt} values were larger than those for acetic$^-$, formic$^-$, F^- and Cl^- ions that were evaluated to have higher charge densities. The three anion species with low charge densities can stay around hydrophobic groups more than the other monovalent anions, thereby hindering hydrophobic contact between the particles, as explained in the preceding paragraph. Thus, the relatively large values of A_{ppt} for thiocyanic ion, iodic ion and nitric ion are related to their ability to hinder mutual contact of hydrophobic groups.

3.2.5. Influences of different cations on the interaction between Rb. shaeroides LH2/OG particle and PEG molecule

The slope of a PC represents the extent of easiness in ejecting PEG molecules from the interparticle space. For instance, when an attractive effect dominates between a particle and a PEG molecule, the slope is gentle; when a repulsive effect dominates, the slope is steep [8]. Here, we note that the standard errors of slope B_{ppt}, evaluated in the least-square fittings of individual PCs and the statistical analysis about the ten PCs (cf. Table 1), are similar to or smaller than the size of symbols in the figure.

The value of B_{ppt} did not significantly vary among the nitrates comprised of different cations. This result is attributable to the symmetrical distribution of electric charges in the cations. Nevertheless, the value of B_{ppt} increased in the order K^+ (0.078) $\leq$ NH_4^+ (0.079) $<$ Li^+ (0.083) $<$ Ca^{2+} (0.086) $\leq$ Mn^{2+} (0.087) $<$ Na^+ (0.089) $=$ Ni^{2+} (0.089) $\leq$ Mg^{2+} (0.090) $\leq$ Cd^{2+} (0.091) $<$ Co^{2+} (0.101) $<$ Zn^{2+} (0.104) (Fig. 1A); there was a tendency that the values of B_{ppt} for divalent cations would be larger than those for monovalent cations. If it is taken into consideration that PEG molecules contain a large number of hydrophobic moieties, this tendency is reasonable because of the following reason. The salt concentrations employed for monovalent cations were higher by a factor of ten in molarity than those for divalent

https://doi.org/10.1016/j.heliyon.2018.e01073

cations. Hence, the particle−PEG hydrophobic 'attraction' in the presence of monovalent cations should be stronger than that in the presence of divalent cations. Moreover, since even divalent cations were not strongly attracted to PEG molecules possessing no distinct charge, such strong attractive effects of divalent cations as induced in the particle−particle interaction should not be induced in the particle−PEG interaction. The affinity of particles to water becomes rather high by the mediation of divalent cations. Thus, the order of ions along the ascending B_{ppt} differs from that along the ascending A_{ppt}, due to the difference in the electrical property between the particle and a PEG molecule.

3.2.6. Influences of different anions on interaction between Rb. shaeroides LH2/OG particle and PEG molecule

For potassium salts comprised of different anions, the value of B_{ppt} increased in the following order: oxalic^{2-} (0.063) $\leq$ F^- (0.064) $<$ acetic$^-$ (0.067) $=$ citric^{3-} (0.067) $\leq$ tartric^{2-} (0.069) $=$ formic$^-$ (0.069) $\leq$ Cl^- (0.070) $<$ SO_4^{2-} (0.077) $\leq$ NO_3^- (0.078) $<$ I^- (0.086) $\leq$ SCN^- (0.088) $<$ HPO_4^{2-} (0.092) (Fig. 1B). This order is interpreted in terms of short-range steric repulsion and hydrophobic 'attraction' whose strength varies depending on the anionic species, as below.

The values of B_{ppt} for NO_3^-, SCN^-, and I^- were larger than those for the other monovalent anions. The interaction of these anions with water molecules is very weak, as shown by the fact that they are not constantly hydrated [25]. Therefore, the ability of short-range steric repulsion in which hydrophilic groups are involved does not differ to a large extent depending on the anionic species. On the other hand, the anions can approach hydrophobic groups around which networks of water molecules are disrupted by the action of potassium ions, and then the anions can stay there due to their weak propensity to move into the aqueous phase. Thus, particle−PEG hydrophobic contact is hindered by the anions whose surface charge density is low. Moreover, when the ion−water interaction strengthens up to the same level as the water−water interaction, ions tend to move into the aqueous phase where they can be surrounded by more water molecules. It follows that the number of ions around hydrophobic groups decreases. Thus, when the ion−water interaction strengthens, the particle−PEG hydrophobic 'attraction' strengthens more than the particle−PEG short-range steric repulsion, as exemplified by the variation of A_{ppt} for halide ions.

The values of B_{ppt} for the five carboxylic ions were smaller than those for Cl^-, I^-, NO_3^- and SCN^- whose interaction with water is very weak [25]. This relationship implies that the angle-averaged interaction between the carboxylic ions and water molecules is closer to the water−water interaction in strength than that of Cl^-, I^-, NO_3^- and SCN^-. There was no significant difference between the values of B_{ppt} for the carboxylic ions of which the number of carboxyl groups is not the same.

https://doi.org/10.1016/j.heliyon.2018.e01073

This result is reasonable, because carboxyl groups mutually separated in multivalent ions interact with hydrophilic groups or solvent molecules to some extent independently of one another, in addition to the fact that the total number of carboxyl groups in the solution is the same in all cases. Moreover, the B_{ppt} for the carboxylic ions increased with an increase in the number of their hydroxyl groups. Hydroxyl groups do not interact with hydrophilic groups or water molecules so strongly as ionized carboxyl groups. Nevertheless, when hydrophilic groups interact with hydroxyl groups of carboxylic ions, they become more difficult to get in contact with other groups. Thus, the number of hydroxyl group in the carboxylic ions also affects B_{ppt} value.

The value of B_{ppt} for HPO_4^{2-} was larger than that for SO_4^{2-}, unlike the dependence of B_{ppt} on ionic species whose interaction with water was comparable to or weaker than the water−water interaction. These two anions HPO_4^{2-} and SO_4^{2-} interact relatively strongly with a hydrophilic molecule and/or a part of a molecule such as charged groups, polar groups and water molecules. When the ionic species is changed from SO_4^{2-} to HPO_4^{2-}, the steric repulsion relevant to hydrophilic groups can strengthen more than the hydrophobic 'attraction', as explained in terms of the influence of cations on the particle−PEG interaction. Thus, when the ion−water interaction exceeds the water−water interaction in strength, the dependence of B_{ppt} on the surface charge density of ions is reversed. It is noted that this dependency makes it difficult to recognize the correlation between the value of B_{ppt} and the electrical properties of ions.

Moreover, the value of B_{ppt} for HPO_4^{2-} is too large to explain the strong effect of the ion in strengthening hydrophobic 'attraction' [10]. It is known that phosphate ions frequently form hydrogen bonds with free NH groups at amino ends of α-helices, due to the favorable geometry in addition to relatively strong dipole moments aligning with the α-helices. This relatively strong interaction seems to manifest itself through the large values of A_{ppt} and B_{ppt} for HPO_4^{2-}. Thus, the extent of effect of ions as steric hindrance in the particle−particle and particle−PEG contact is also related to the geometrical arrangement of oxygen atoms in the ions.

3.2.7. Horizontal position of PC of Rb. shaeroides LH2/OG for various ions

Since the values of B_{ppt} are not the same for all nitrates, a few PCs cross each other on the precipitation diagram. For instance, the PCs for Ni^{2+} and Zn^{2+} cross at the point (62 mg PEG/mL, 14 mg protein/mL) and the PCs for Li^+ and NH_4^+ at the point (112 mg PEG/mL, 36 mg protein/mL). For the same reason, the PC for HPO_4^{2-}, showing the largest B_{ppt}, crossed the PCs for citrate^{3-}, SO_4^{2-} and oxalate^{2-} at the points (180 mg PEG/mL, 17 mg protein/mL), (226 mg PEG/mL, 0.25 mg protein/mL) and (216 mg PEG/mL, 0.65 mg protein/mL), respectively. Thus, the

https://doi.org/10.1016/j.heliyon.2018.e01073

relationship between the horizontal position of PC and the ionic species is changed depending on the values of supernatant protein concentrations to be used. To avoid such ambiguity, the PEG concentration $[P]_5$ at which the protein concentration is 5 mg/mL in a supernatant is defined as the horizontal position of a PC hereafter. Another reason for the choice of $[P]_5$ is because the value of $[P]_5$, roughly corresponding to the midpoint of measurement range, is a practical indicator to represent the behavior of a PC.

The standard errors of $[P]_5$, evaluated in the least-square fittings of individual PCs and the statistical analysis about the ten PCs (cf. Table 1), were similar to or smaller than the size of symbols in the figure. The values of $[P]_5 = (A_{ppt} - ln\ 5)/B_{ppt}$ for nitrates and potassium salts line up in the order Cd^{2+} (57.4 mg/mL) < Zn^{2+} (71.9 mg/mL) < Ni^{2+} (73.5 mg/mL) < Co^{2+} (83.2 mg/mL) < Mn^{2+} (94.9 mg/mL) < Ca^{2+} (111.5 mg/mL) < Mg^{2+} (114.9 mg/mL) < Na^{+} (125.6 mg/mL) < Li^{+} (136.2 mg/mL) < NH_4^{+} (137.4 mg/mL) < K^{+} (143.3 mg/mL) and in the order SCN^{-} (123.3 mg/mL) < I^{-} (125.8 mg/mL) < NO_3^{-} (143.3 mg/mL) < Cl^{-} (148.4 mg/mL) < formic^{-} (150.7 mg/mL) < acetic^{-} (155.3 mg/mL) < tartric^{2-} (164.5 mg/mL) < F^{-} (168.5 mg/mL) < oxalic^{2-} (183.3 mg/mL) < SO_4^{2-} (187.2 mg/mL) < HPO_4^{2-} (193.6 mg/mL) < citric^{3-} (198.4 mg/mL) along the PEG concentration, respectively. These orders of ions along the ascending $[P]_5$ exhibit the following features. First, the variation of $[P]_5$ with ionic charge number is opposite in the cases of cations and anions. Second, the effectiveness of divalent cations, employed as precipitants in combination with PEG, increases with increasing atomic number. Moreover, the effectiveness of anions is opposite to the effectiveness in salting-out of macromolecules in the case of employment of salts without PEG, that is, the so-called 'lyotopic series' [10, 11].

3.3. Dependence of PC on cationic and anionic species of *Rb. sphaeroides* LH2 solubilized by OG, LDAO and $C_{12}E_8$

With *Rb. sphaeroides* LH2/OG, the variation of PC for various nitrates and potassium salts is related to the effects of ions that vary depending on the ionic properties. To investigate whether the relationship would be valid for salts of other ionic pairs, PCs for various salts were determined for *Rb. sphaeroides* LH2 separately solubilized by three kinds of detergents (OG, *N*,*N*−dimethyldodecylamine−*N*−oxide (LDAO) and *N*−dodecyl−octaoxyethylene ($C_{12}E_8$)) whose hydrophilic head groups are of different types [8]. Here, salts comprised of multivalent cations and multivalent anions were not examined except sulfates, because their employment is limited due to the low solubility in water.

Fig. 2 shows the result of *Rb. sphaeroides* LH2/OG; the values of A_{ppt}, B_{ppt} and $[P]_5$ are shown as a histogram for cationic and anionic species at 0.4 M for 1:1 salts, 0.2 M for 1:2 ones, 0.133 M for 1:3 ones, and 0.04 M for 2:1 and 2:2 ones. For the

https://doi.org/10.1016/j.heliyon.2018.e01073

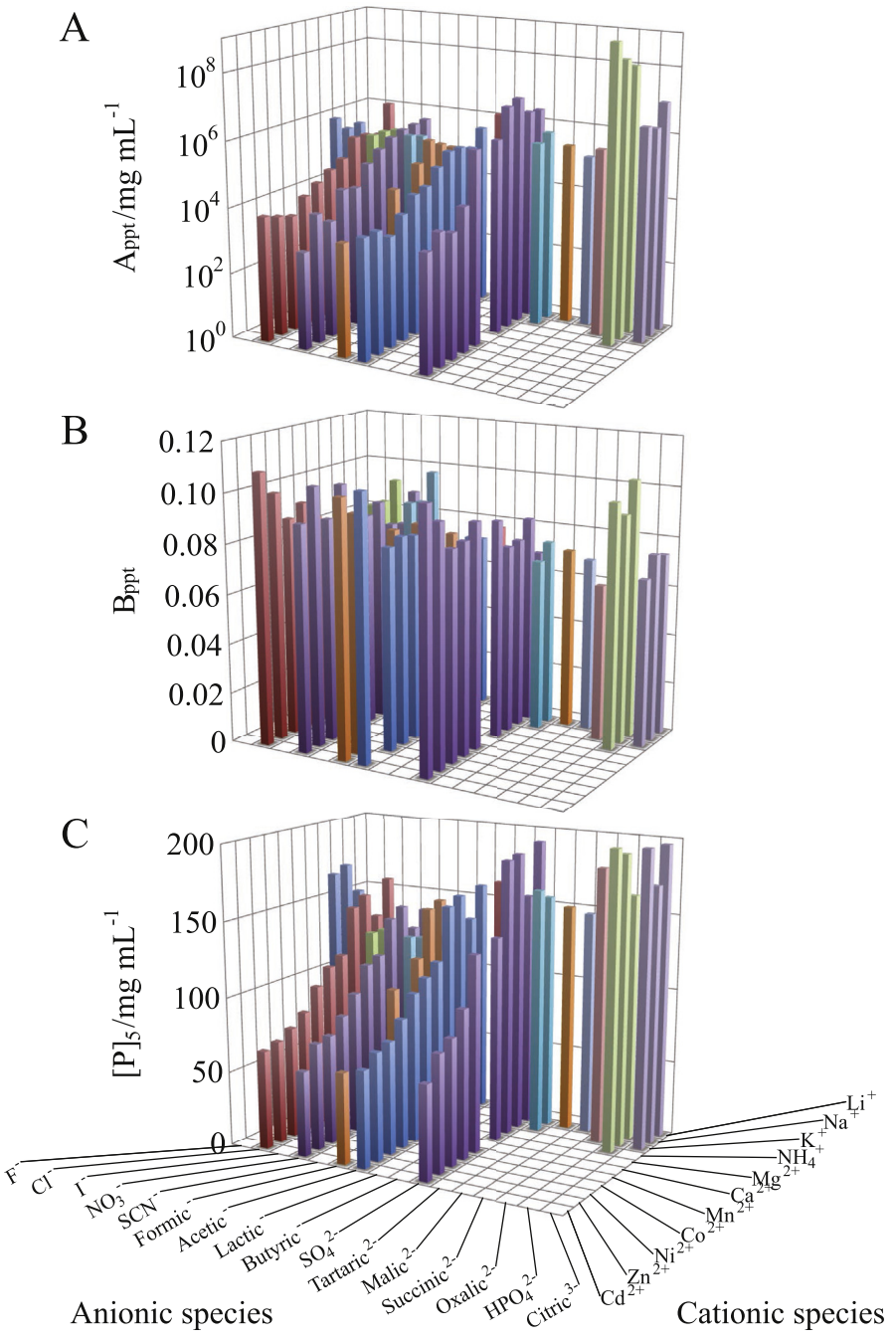

Fig. 2. Dependence of PC of *Rb. sphaeroides* LH2/OG on constituent cationic and anionic species of the salts added. The values of (A) intercept A_{ppt}, (B) slope B_{ppt} and (C) horizontal position $[P]_5$ (PEG concentration at which the protein concentration $[D]_{ppt}$ in supernatant was 5 mg/mL) were based on the best-fitted PCs. The concentrations of added salts were 0.4 M for 1:1 salts, 0.2 M for 1:2 ones, 0.133 M for 1:3 ones, and 0.04 M for 2:1 and 2:2 salts. The other solution ingredients were 25 mM Tris−HCl (pH 8.0), 0.2 mg/mL NaN_3, and 8 mg/mL OG.

https://doi.org/10.1016/j.heliyon.2018.e01073

various salts, each of the three parameters exhibited basically the same dependence on cationic and anionic species as that described above. This result indicates that the anions and cations do not strongly interfere with each other in their action on the particles and PEG molecules. The results of LDAO and $C_{12}E_8$ particles (shown in Figs. 3 and 4, respectively) do not show any indication of a strong ion-pair effect, either. Such a weak ion-pair effect allows us to deal with the effects of cations and anions separately.

The dependence of A_{ppt} on ionic species was similar between the OG particle (Fig. 2A) and the LDAO one (Fig. 3A), but the $C_{12}E_8$ particle showed different variation for salts comprised of monovalent cations (Fig. 4A). Moreover, when the atomic number of divalent cation was increased, the B_{ppt} of OG particle (Fig. 2B) and LDAO one (Fig. 3B) tended to increase, but the $C_{12}E_8$ particle exhibited the opposite tendency (Fig. 4B). Thus, each dependence of A_{ppt} and B_{ppt} on ionic species was not the same among the three kinds of particles. However, the relationship between the $[P]_5$ and the ionic species was analogous among the three kinds of particles (cf. Figs. 2C, 3C and 4C). This means that the $[P]_5$ can be expressed as a simple additive function of cationic and anionic species.

To deduce the function, ratios of $[P]_5$ for the other cationic species to $[P]_5$ for K^+ were calculated regarding the PCs for the salts composed of the same anionic species, and then the ratios were averaged over all anionic species. Likewise, the ratios of $[P]_5$ for the other anionic species to $[P]_5$ for NO_3^- were averaged over all cationic species. The ratios $S_{\pm}$ calculated for various ionic species are listed in Table 2. When these values S_+ and S_- are used as parameters to specify constituent cationic and anionic species of the salt added, respectively, the horizontal position $[P(S_+, S_-)]_5$ for the salt is related to the values of S_+ and S_-, through the following equation,

$$[P(S_+, S_-)]_5 = F\,S_+ + G\,S_- + H \tag{2}$$

here, F, G, and H are constants for the individual particles.

3.4. Dependence of PC on ionic species of *Rb. sphaeroides* LH2 solubilized by different types of detergents

3.4.1. Rb. sphaeroides LH2 solubilized by detergents with a ring−shaped sugar head

To explore wider applicability of Eq. (2), dependence of PC on ionic species was further investigated about other protein/detergent particles. It was expected that the PCs of *Rb. sphaeroides* LH2 would strongly reflect the property of the detergent cluster around the protein molecule, due to the small extramembraneous region of the protein [8]. With *Rb. sphaeroides* LH2 separately solubilized by the detergents

https://doi.org/10.1016/j.heliyon.2018.e01073

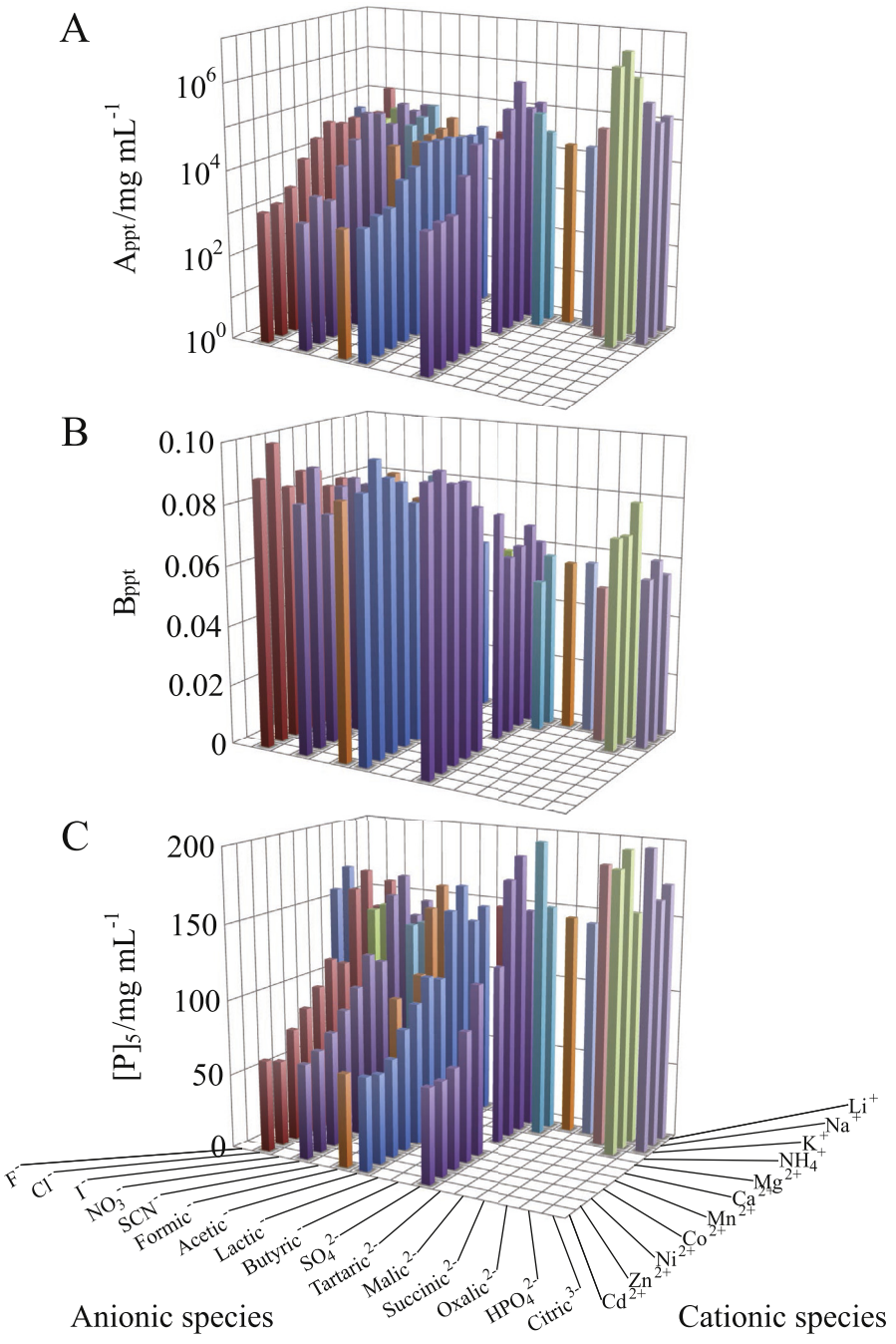

Fig. 3. Dependence of PC of *Rb. sphaeroides* LH2/LDAO on constituent cationic and anionic species of the salts added. The values of (A) intercept A_{ppt}, (B) slope B_{ppt} and (C) horizontal position $[P]_5$ were based on the best-fitted PCs. The concentrations of added salts were 0.4 M for 1:1 salts, 0.2 M for 1:2 ones, 0.133 M for 1:3 ones, and 0.04 M for 2:1 and 2:2 salts. The other solution ingredients were 25 mM Tris−HCl (pH 8.0), 0.2 mg/mL NaN_3, and 1 mg/mL LDAO.

https://doi.org/10.1016/j.heliyon.2018.e01073

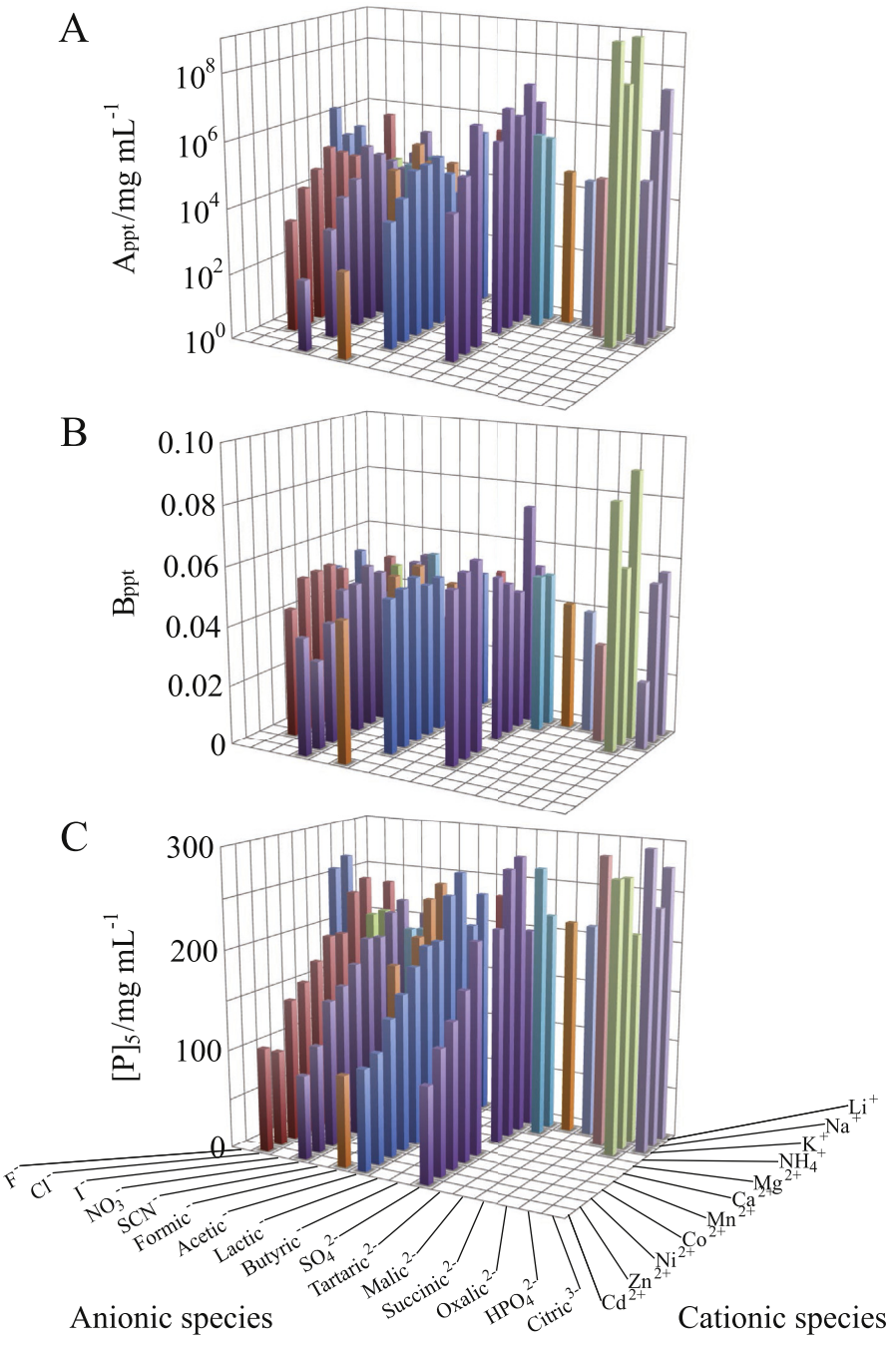

Fig. 4. Dependence of PC of *Rb. sphaeroides* LH2/$C_{12}E_8$ on constituent cationic and anionic species of the salts added. The values of (A) intercept A_{ppt}, (B) slope B_{ppt} and (C) horizontal position $[P]_5$ were based on the best-fitted PCs. The concentrations of added salts were 0.4 M for 1:1 salts, 0.2 M for 1:2 ones, 0.133 M for 1:3 ones, and 0.04 M for 2:1 and 2:2 salts. The other solution ingredients were 25 mM Tris−HCl (pH 8.0), 0.2 mg/mL NaN_3, and 1 mg/mL $C_{12}E_8$. Since the supernatant protein concentrations in the presence of $ZnCl_2$, $Zn(CH_3COO)_2$, $ZnSO_4$, $CdCl_2$, $Cd(CH_3COO)_2$, or $CdSO_4$ followed the equation $[D]_{ppt} = A_{ppt} - B_{ppt}[P]$, the B_{ppt} values for the salts are not shown. Hence, further investigations are awaited to elucidate the molecular mechanism concerning the linear variation between $[D]_{ppt}$ and [P].

https://doi.org/10.1016/j.heliyon.2018.e01073

Table 2. Relative positions of PCs of *Rb. sphaeroides* LH2 particles for constituent cations and anions of salts added.

Cation	S_+	Anion	S_-
Li^+	0.93	F^-	1.12
Na^+	0.83	Cl^-	1.02
K^+	1.00	I^-	0.92
NH^{4+}	0.97	$NO3^-$	1.00
Mg^{2+}	0.74	SCN^-	0.89
Ca^{2+}	0.74	$Formic^-$	1.03
Mn^{2+}	0.67	$Acetic^-$	1.03
Co^{2+}	0.57	$Lactic^-$	1.11
Ni^{2+}	0.49	$Butyric^-$	1.06
Zn^{2+}	0.42	$SO4^{2-}$	1.15
Cd^{2+}	0.39	$Tartric^{2-}$	1.21
		$Malic^{2-}$	1.14
		$Succinic^{2-}$	1.23
		$Oxalic^{2-}$	1.16
		$HPO4^{2-}$	1.25
		$Citric^{3-}$	1.32

indicated in the caption to Fig. 5, the values of A_{ppt}, B_{ppt} and $[P]_5$ are plotted against $S_\pm$ in Fig. 5. Even if the influences of the two kinds of standard errors were taken into consideration, the fitted values of A_{ppt} and B_{ppt} did not seem to vary linearly against $S_\pm$ (Fig. 5A, B, D and E). However, the $[P]_5$ of each particle varied linearly against $S_\pm$, as expected in the preceding paragraph; the deviations of $[P]_5$ from the line, which was calculated by least-square fitting of a linear function to the experimental values of $[P]_5$, were mostly within $\pm$10 mg/mL in terms of PEG concentration (Fig. 5C and F). We will consider why the linear relationship between $[P]_5$ and $S_\pm$ arises from the nonlinear variations of A_{ppt} and B_{ppt} with $S_\pm$, in the following paragraphs.

OG, *N*−octyl−β−*D*−thioglucoside (OTG), β−*D*−fructopyranosyl−α−*D*−glucopyranoside monododecanoate (SML), LM, and *N*−nonyl−β−*D*−thiomaltoside (NTM) have a ring-shaped sugar as a polar head. These detergents are referred to as RSH in this study. The variation of A_{ppt} with $S_\pm$ (Fig. 5A and D) was analogous among the *Rb. sphaeroides* LH2/RSHs (black symbols), though the values themselves of A_{ppt} differed depending on the number of hydroxyl groups at the polar heads of RSHs [8]. The variation of B_{ppt} with $S_\pm$ (Fig. 5B and E) was also analogous among the five kinds of particles. These results mean that the influences of ions on the particle−particle and particle−PEG interactions are basically the same as explained in the case with *Rb. sphaeroides* LH2/OG. Moreover, the

https://doi.org/10.1016/j.heliyon.2018.e01073

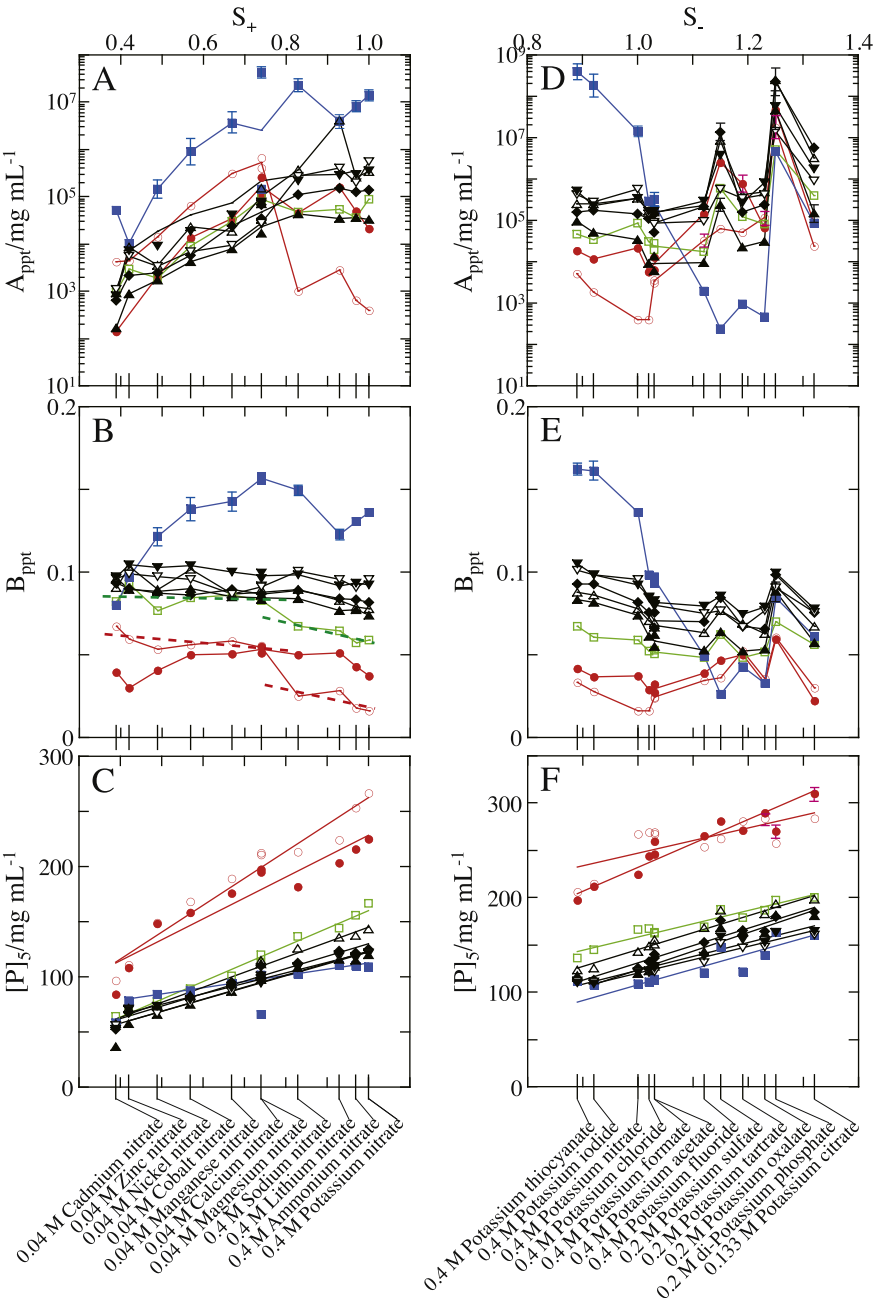

Fig. 5. Variation of PC for ionic species observed with *Rb. sphaeroides* LH2 separately solubilized by nine species of detergents. A − C; the added salts were nitrates of various cations, and the salt concentrations were 0.4 M for 1:1 salts and 0.04 M for 2:1 and 2:2 ones. D − F; the added salts were potassium salts of various anions, and the salt concentrations were 0.4 M for 1:1 salts, 0.2 M for 1:2 ones, 0.133 M for 1:3 salt to equalize the concentration of potassium ion. The values of (A and D) intercept A_{ppt}, (B and E) slope B_{ppt} and (C and F) horizontal position $[P]_5$ of the best-fitted PCs are plotted against the $S_{\pm}$ values allotted to the constituent ionic species. The solubilization detergents and their concentrations were 1 mg/ml TX100 (◯), 1 mg/ml $C_{12}E_8$ (●), 1 mg/ml LDAO (□), 9 mg/ml MEGA9 (■), 8 mg/ml OG (△), 1 mg/ml LM (▽), 1 mg/ml SM1200 (◆), 3 mg/ml OTG (▲), and 2 mg/ml NTM (▼). The other solution ingredients were 25 mM Tris−HCl (pH 8.0) and 0.2 mg/mL NaN_3. The straight lines

https://doi.org/10.1016/j.heliyon.2018.e01073

similar variations in individual parameters among the five kinds of particles are also the reason for their linear relationships between $[P]_5$ and $S_{\pm}$ (Fig. 5C and F), because Eq. (2) is based on the results of the three kinds of particles including *Rb. sphaeroides* LH2/OG.

It is likely that PEG molecules, polymers of $-OCH_2CH_2-$ repeat units, shrink to some extent by addition of a salt, because their intramolecular hydrophobic interactions are strengthened by addition of a salt, as is the case with oligo−oxyethylene head detergents [30]. Moreover, it is suggested that the effect of PEG as a precipitant weakens with decreasing PEG size [31, 32]. In fact, such a variation was observed for human serum albumin [33]. Therefore, the value of B_{ppt} is expected to decrease with salt concentration. However, when ionic species was changed from divalent cations to monovalent ones, that is, when the salt concentration was raised from 0.04 M to 0.4 M, the B_{ppt} of *Rb. sphaeroides* LH2/RSHs did not noticeably decrease (Fig. 5B). This result means that the shrinkage of PEG molecules has only a negligible influence on the particle−PEG interaction, as compared with the direct influence of ions.

3.4.2. *Rb. sphaeroides* LH2 solubilized by MEGA9

Nonanoyl−*N*−methylglucamide (MEGA9) and OG have the same number of hydroxyl groups at their polar heads. However, variations of both A_{ppt} and B_{ppt} with S_{+} were not the same between *Rb. sphaeroides* LH2/MEGA9 (blue symbols in Fig. 5) and *Rb. sphaeroides* LH2/OG. For the nitrates, the A_{ppt} and B_{ppt} of MEGA9 particle exhibited obviously larger values and variations than those of OG particle (Fig. 5A and B). For KSCN, KI and KNO_3, the A_{ppt} and B_{ppt} of MEGA9 particle also exhibited obviously large values in comparison with the corresponding parameters of OG particle (Fig. 5D and E). These large values and variations are attributable to the high density of hydroxyl groups in the hydrophilic layer of the detergent cluster in which MEGA9 molecules are tightly packed in the presence of salts such as NaCl, KNO_3 and $Mg(NO_3)_2$ [8,34].

The A_{ppt} and B_{ppt} of *Rb. sphaeroides* LH2/MEGA9 exhibited smaller values for multivalent anions, especially for divalent anions such as SO_4^{2-}, tartraric^{2-} and oxalic^{2-}, than those of *Rb. sphaeroides* LH2/OG. Thus, the two parameters of MEGA9 particle varied irregularly with the ionic charge number. This means that the difference in the ionic charge is not a major origin for the irregular variation. However, the reason can be interpreted by considering the difference in the ionic

were obtained by the least-squares fitting of a linear function to the value of $[P]_5$ against the value of $S_{\pm}$ to show the mean variation of PC depending on ionic species. The error bars attached to symbols represent standard errors calculated by the least-square fitting; no error bar is shown for the standard errors that are similar to or smaller than the size of symbols. Besides, it is noted that the maximal standard errors shown in Table 1 are similar to or smaller than the size of symbols.

https://doi.org/10.1016/j.heliyon.2018.e01073

size, as follows. Whereas hydrated trivalent anions are too large to be accommodated in the space between MEGA9 polar heads, hydrated divalent anions can barely be done. The accommodated divalent anions, due to their comparatively large size, disorder and loosen the packing of MEGA9 polar heads in the detergent cluster [8], resulting in lowering the density of water molecules and ions attractively interacting with the detergent cluster surface. Thus, the strength and range of steric repulsion can be particularly weak in the presence of divalent anions.

When ionic species was changed along the ascending $S_{\pm}$, the A_{ppt} and B_{ppt} of *Rb. sphaeroides* LH2/MEGA9 simultaneously increased or decreased. Such synchronous variation of A_{ppt} and B_{ppt} partially canceled their opposing influences on variation of $[P]_5$. As a result, the linear relationship between $[P]_5$ and $S_{\pm}$ was maintained (Fig. 5C and F) even for *Rb. sphaeroides* LH2/MEGA9 whose state seemed to vary depending on the ionic species.

3.4.3. *Rb. sphaeroides LH2 solubilized by oligo−oxyethylene detergents*

The polar heads of TX100 (*T*−octylphenoxypolethoxyethanol) and $C_{12}E_8$ molecules are constituted of the same repeat unit $-OCH_2CH_2-$. However, *Rb. sphaeroides* LH2/TX100 and *Rb. sphaeroides* LH2/$C_{12}E_8$ (red symbols in Fig. 5) exhibited the following differences in variations of both A_{ppt} and B_{ppt} with S_-. When cationic species was changed from Mg^{2+} to Na^+, the A_{ppt} (Fig. 5A) and B_{ppt} (Fig. 5B) of TX100 particle discontinuously decreased, but such a decrease was not observed in the variations of A_{ppt} and B_{ppt} of $C_{12}E_8$ particle. Moreover, in the case of potassium salts whose concentrations were of the order of hundreds mM, the variations of both A_{ppt} and B_{ppt} with S_- were analogous between TX100 particle and $C_{12}E_8$ one. These results imply that the large decrease in the two parameters of TX100 particle is involved in some change in the state of TX100 cluster that is caused by variation in the concentration rather than the salt species added. In our previous study [8], it was shown that when hydrophobic 'attraction' was strengthened with increasing salt concentration, the surface of a TX100 cluster could become larger and more uneven, due to the bulky and inflexible hydrophobic moiety of a TX100 molecule. Such change in the TX100 cluster appears to be reflected as the large decrease in A_{ppt} and B_{ppt}.

The A_{ppt} (Fig. 5D) and B_{ppt} (Fig. 5E) of TX100 particle exhibited a trough over NO_3^- to Cl^- in their variations with S_-. However, such a trough was not observed for $C_{12}E_8$ particle. The troughs in the variations of A_{ppt} and B_{ppt} of TX100 particle seem to reflect some variation in the detergent cluster for NO_3^- and Cl^-. However, more precise comprehension of the mechanism needs further investigations.

With respect to variations of A_{ppt} and B_{ppt} with $S_{\pm}$, $C_{12}E_8$ particle was similar to RSH ones rather than TX100 particle. This similarity seems to reflect the structural

https://doi.org/10.1016/j.heliyon.2018.e01073

similarity between $C_{12}E_8$ molecule and RSHs ones. The hydrophobic tails of $C_{12}E_8$ and RSHs are neither so bulky nor so inflexible as the hydrophobic moiety of TX100. Hence, before the addition of salts $C_{12}E_8$ molecules are already more densely packed within the cluster than TX100 molecules. Within the $C_{12}E_8$ cluster that is already stuffed with the detergent molecules, the molecular packing is difficult to be further tightened depending on the concentration and salt species added.

Although the values themselves of A_{ppt} and B_{ppt} differed between $C_{12}E_8$ particle and OG one, their variations with $S_{\pm}$ were analogous between the two kinds of particles, as mentioned in the preceding paragraph. For this reason, the $[P]_5$ of $C_{12}E_8$ particle linearly varied with $S_{\pm}$ as well as that of OG particle (Fig. 5C and F). By contrast, in spite of the irregular variations of A_{ppt} and B_{ppt} for several ionic species, the TX100 particle exhibited a comparatively good linear relationship between $[P]_5$ and $S_{\pm}$ (Fig. 5C and F). This is attributed to the synchronous variation of A_{ppt} and B_{ppt} that partially cancel their opposing influences on the variation of $[P]_5$.

3.4.4. Rb. sphaeroides LH2 solubilized by LDAO

When monovalent cationic species was changed along the ascending S_+, the A_{ppt} of *Rb. sphaeroides* LH2/LDAO (green symbols in Fig. 5) exhibited neither an appreciable increase nor a decrease (Fig. 5A). This result can be interpreted as follows. The polar head of LDAO molecule has two hydrophobic methyl groups in addition to a dipole moment along the N−O bond. Electric repulsion among the mutually 'parallel' dipole moments (in the sense that they tend to point in the inward direction of the detergent cluster) and hydrophobic 'attraction' based on the methyl groups work simultaneously among the heads in the directions along the surface of the detergent cluster. The electric repulsion is weakened and the hydrophobic 'attraction' is strengthened by addition of a salt. These variations in the head−head interaction not only increase the aggregation number of LDAO molecules in the cluster [8] but also compress the cluster even more tightly. As a result, the densities of N−O bonds and methyl groups increase at the same ratio in the hydrophilic layer of the detergent cluster. Thus, the hydrophilic 'repulsion' and the hydrophobic 'attraction' are strengthened to the same extent in the particle−particle interaction. This seems to be reflected as the nearly constant value of A_{ppt}.

When cationic species was changed from Mg^{2+} to Na^+, the B_{ppt} of LDAO particle discontinuously decreased (Fig. 5B); the B_{ppt}−S_+ line for monovalent cations was below that for divalent cations (cf. two green dotted lines). This decrease in B_{ppt} is not attributable to the particle−PEG hydrophobic 'attraction' strengthening with salt concentration, due to the reason explained in the preceding paragraph. However, if the polar−nonpolar distribution on the particle surface resembles that on the PEG surface, then the particle can have a high affinity to a PEG molecule, for the following reason. The amine oxide moieties and methyl groups of LDAO heads

https://doi.org/10.1016/j.heliyon.2018.e01073

are alternately arranged in the hydrophilic layer of the detergent cluster so as to lower their interaction energy. When the LDAO heads are more tightly packed, the periodic length of polar−nonpolar arrangement ($-NO-CH_3\cdots H_3C-$) on the cluster surface approaches that ($-OCH_2CH_2-$) on the PEG surface, resulting in a higher affinity between the two surfaces. In addition, LDAO molecules tend to form a cluster with a surface of smaller curvature, because of the small ratio in size of polar head−to−hydrophobic tail. This tendency becomes stronger with the salt concentration, because of the decrease in the repulsive forces between mutually 'parallel' dipole moments. As a result, the effective contact area between the detergent cluster surface and the PEG surface becomes larger. Such variations in the state of a LDAO cluster can cause a large decrease of B_{ppt}. Thus, the large decrease of B_{ppt} is related to a closer packing of LDAO molecules in the cluster.

When cationic species was changed along the ascending S_+, the A_{ppt} of LDAO particle increased for divalent cations but was nearly constant for monovalent cations (Fig. 5A). On the other hand, the down slope of B_{ppt} plotted against S_+ was steeper for monovalent cations than for divalent cations (Fig. 5B). As a result, the variations of $[P]_5$ for monovalent cations and divalent ones were continuously joined together (Fig. 5C), resulting in the linear relationship between $[P]_5$ and S_+. For anions, the variations of A_{ppt} and B_{ppt} with S_- were basically the same for LDAO particle and OG one (Fig. 5D and E). Due to such similar variations between the two kinds of particles, the $[P]_5$ of LDAO particle varied linearly with S_- (Fig. 5F), as was the case with OG particle.

3.5. Dependence of PC of different integral membrane proteins on the ionic species

3.5.1. Rb. sphaeroides and Rb. capsulatus LH2s solubilized by LM

Fig. 6 shows the variations of A_{ppt}, B_{ppt} and $[P]_5$ with $S_\pm$ observed for *Rp. viridis* PRU and RC, *Rb. sphaeroides* RC and LH2, and *Rb. capsulatus* LH2. In this experiment, LM was mainly used as a solubilization detergent, because LM cluster held each of the five proteins in a comparatively stable state [5, 8, 9, 35] and because there was no indication of significant variation in packing state of LM molecules in *Rb. sphaeroides* LH2/LM.

Rb. sphaeroides LH2 and *Rb. capsulatus* LH2 are similar to each other in the primary structure [24, 36, 37] besides the molecular weight, Stokes radius, pI and extramembranous surface area. However, the variation of solubility with ammonium sulfate concentration is quite different between the two LH2s [9] due to the difference in their amino acid compositions of extramembranous regions [8, 23, 38]. With *Rb. sphaeroides* (red symbols) and *Rb. capsulatus* LH2s (blue symbols), the

https://doi.org/10.1016/j.heliyon.2018.e01073

A_{ppt} exhibited local maxima for SO_4^- and HPO_4^{2-} in the variation against S_- (Fig. 6D and E); the values of A_{ppt} for these anionic species were larger than those for their neighboring anionic species in terms of S_- (F^- and tartric^{2-} for SO_4^-, and oxalic^{2-} and citric^{3-} for HPO_4^{2-}). However, such obvious local maxima were not observed with the other three kinds of proteins. This suggests that the local maxima are attributed to not only the relatively strong electric fields of the anions but also some property of LH2s. Due to the structural feature [36, 37] that both LH2s are composed of 18 transmembrane α-helices aligning in the same direction, relatively strong electric fields, pointing to the direction along the α-helices, are generated around both ends of the α-helices [8]. It follows that SO_4^- and HPO_4^{2-} attracted to the extra-micellar regions hinder association of LH2 particles. Thus, the local maxima of A_{ppt} seem to reflect the relatively strong interactions between the ions and the LH2s.

When cationic species was changed from Mg^{2+} to Na^+ along the ascent of S_+, the A_{ppt} and B_{ppt} of *Rb. sphaeroides* LH2/LM discontinuously increased (Fig. 6A and B). However, such discontinuous increases were not observed with *Rb. capsulatus* LH2. Moreover, the A_{ppt} and B_{ppt} of *Rb. sphaeroides* LH2 exhibited larger local maxima for HPO_4^{2-} than the corresponding parameters of *Rb. capsulatus* LH2 (Fig. 6D and E). These differences between the two kinds of LH2s cannot be explained in terms of the electric field from α-helices and the hydrophobic 'attraction'. This is because the electric field from their α-helices are considered comparable in strength between the two kinds of LH2s [8] and because *Rb. sphaeroides* LH2 that has a larger number of moieties composed of 4 or more consecutive hydrophobic residues in the extra-micellar region than *Rb. capsulatus* LH2 [24,36].

However, the number of ions to hinder the particle-particle contact differs between the two LH2s because of the difference in the number of charged amino acid residues in the extra-micellar regions [24, 38]. For instance, *Rb. sphaeroides* LH2 has a glutamic acid (with two carboxyl groups) at the C-terminus of each α-polypeptide, whereas *Rb. capsulatus* LH2 has no ionizable residues in the extra-micellar C-terminal region. Therefore, *Rb. sphaeroides* LH2 can attract more monovalent cations than *Rb. capsulatus* LH2. The negative charges of *Rb. sphaeroides* LH2 may also attractively interact with electropositive proton of HPO_4^{2-} (the major form of phosphoric ion at pH 8.0). Besides, the strength and direction of electric fields of the α-helices should be differently modified by electric fields of electric charges and dipoles in the extra-micellar regions whose configuration differs between the two LH2s. However, more precise analysis of the influence needs determination of their detailed structures.

With *Rb. sphaeroides* LH2, the discontinuous increase of A_{ppt} due to the change of cationic species is more distinct than that of B_{ppt} (cf. Fig. 6A and B). As already explained, divalent cations and monovalent cations play basically the same role (steric hindrance) in the particle−PEG contact, though their ability differs. Therefore, the

https://doi.org/10.1016/j.heliyon.2018.e01073

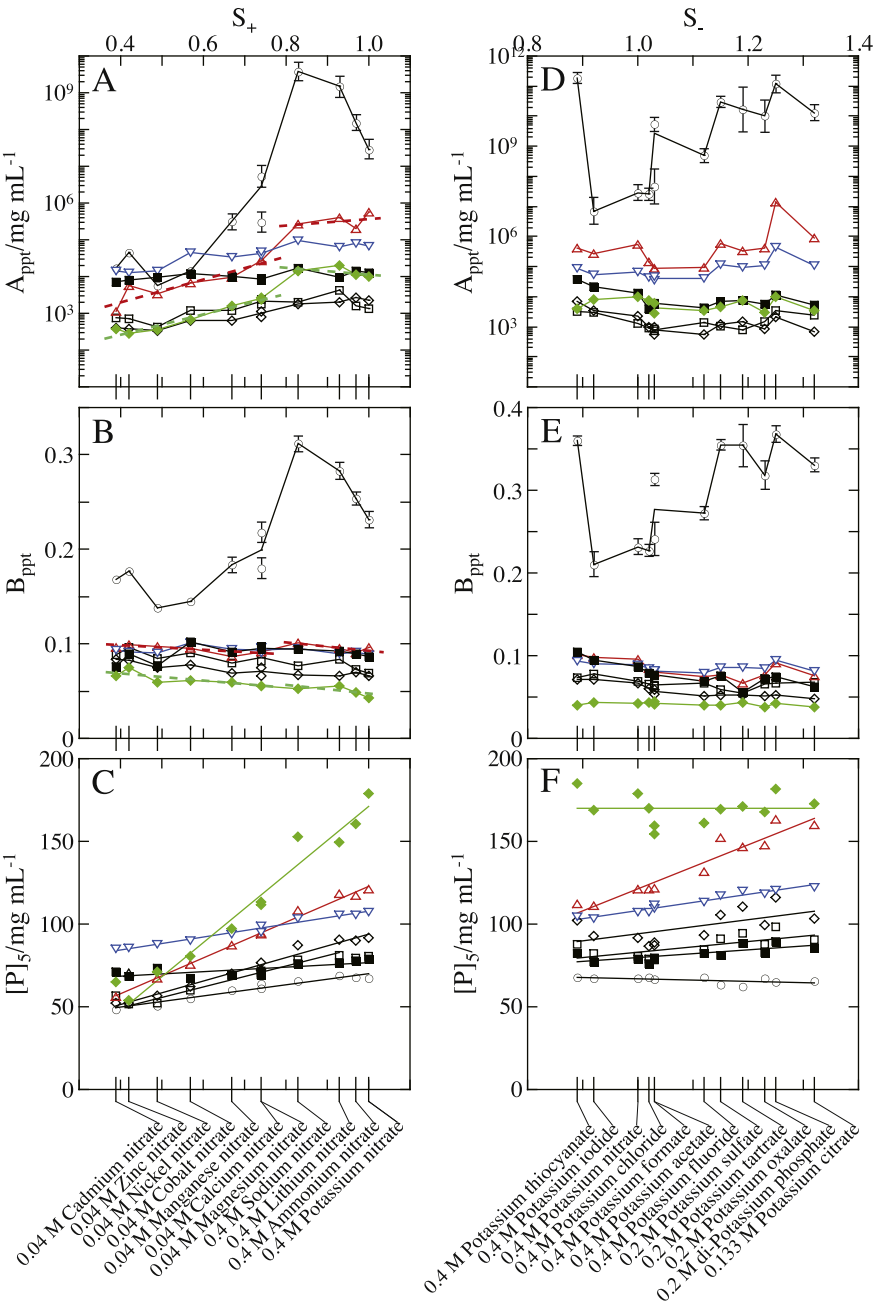

Fig. 6. Variation of PC for ionic species observed with particles of different proteins. A − C; the added salts were nitrates of various cations, and the salt concentrations were 0.4 M for 1:1 salts and 0.04 M for 2:1 and 2:2 ones. D − F; the added salts were potassium salts of various anions, and the salt concentrations were 0.4 M 1:1 salts, 0.2 M 1:2 ones, 0.133 M 1:3 salt to equalize the concentration of potassium ion. The values of (A and D) intercept A_{ppt}, (B and E) slope B_{ppt} and (C and F) horizontal position $[P]_5$ of the best-fitted PCs are plotted against the $S_{\pm}$ values allotted to the constituent ionic species. The protein/detergent particles and solution ingredients were as follows: *Rp. viridis* PRU/LM (◯), *Rp. viridis* RC/LM (□), *Rb. sphaeroides* RC/LM (◇), *Rb. sphaeroides* RC/LDAO (◆), *Rb. sphaeroides* LH2/LM (△) and *Rb. capsulatus* LH2/LM (▽) in a Tris buffer solution (25 mM Tris−HCl, and 0.2 mg/mL NaN_3; pH 8.0), and *Rp. viridis* RC/LM (■) in a BisTris buffer solution (25 mM BisTris−HCl, and

https://doi.org/10.1016/j.heliyon.2018.e01073

strength of particle−PEG interaction is determined by the compromise between steric repulsion and hydrophobic 'attraction' both of which strengthen with salt concentration. By contrast, when divalent cations are replaced by monovalent cations, the role of cation in the particle−particle association changes from a connector to an obstacle. Hence, the particle−particle interaction can vary more significantly in strength than the particle−PEG interaction, causing a larger increase in A_{ppt} than in B_{ppt}. With the two kinds of LH2s, moreover, the local maxima of A_{ppt} for SO_4^- and HPO_4^{2-} were more distinct than those of B_{ppt} (Fig. 6D and E). PEG molecules do not attract so strongly the anions as the particles. On this account, the steric hindrance between the particles and PEG molecules is not so strong all over the interspace as that between the particles. Thus, the influence of steric hindrance is difficult to manifest itself in the particle−PEG interaction so distinctly as in the particle−particle interaction.

With *Rb. capsulatus* LH2/LM, as a result of the A_{ppt} gradually increasing and the B_{ppt} slightly decreasing with S_+, the $[P]_5$ also gradually increased with S_+, leading to a linear relationship between $[P]_5$ and S_+ (Fig. 6C). Moreover, the variations of A_{ppt} and B_{ppt} with S_- draw similar outlines, resulting in a linear relationship between $[P]_5$ and S_- (Fig. 6F). On the other hand, with *Rb. sphaeroides* LH2/LM, the A_{ppt} and B_{ppt} exhibited a simultaneous increase for several ions such as Na^+, SO_4^{2-} and HPO_4^{2-} in their variations with $S_\pm$. However, their offsetting did not make $[P]_5$ vary for the ionic species to a considerable extent, causing the linear relationship between $[P]_5$ and $S_\pm$ (Fig. 6C and F). Such a relationship among A_{ppt}, B_{ppt} and $[P]_5$ has been observed with the other particles in the current study. This is not fortuitous, though irregular variations of A_{ppt} and B_{ppt} arose from different causes. This is because both of the particle−particle and particle−PEG interactions are related with the properties of particles and the state of solvent, and therefore also with their variations. Thus, the linear relationship between $[P]_5$ and $S_\pm$ is maintained by the correlative variations of A_{ppt} and B_{ppt} with $S_\pm$.

3.5.2. *Rp. viridis* PRU solubilized by LM

In *Rp. viridis* PRU, the RC [39, 40, 41, 42, 43] is surrounded by LH1-subunit that is composed of 16 pairs of transmembrane α- and β-polypeptides aligning in the same direction [44, 45, 46]. With *Rp. viridis* PRU/LM in Tris buffer (pH 8.0), the A_{ppt} and B_{ppt} exhibited large values and fluctuations to $S_\pm$ (Fig. 6A, B, D, and E). Such large values and fluctuations were not observed in the case with *Rp. viridis* RC/LM in

0.2 mg/mL NaN_3; pH 6.0). The concentrations of LDAO and LM were 1 mg/mL. The straight lines were obtained by the least-squares fitting of a linear function to the value of $[P]_5$ against the value of $S_\pm$ to show the mean shift of PC depending on ionic species. The error bars attached to symbols represent standard errors calculated by the least-square fitting; no error bar is shown for the standard errors that are similar to or smaller than the size of symbols.

https://doi.org/10.1016/j.heliyon.2018.e01073

BisTris buffer (25 mM BisTris−HCl, and 0.2 mg/mL NaN_3; pH 6.0) (Fig. 6A, B, D, and E), though the deviation of the protein pI value from the solvent pH value was analogous in both cases. This means that the difference in net charge of protein is not a major reason for the large values and fluctuations of the two parameters of *Rp. viridis* PRU/LM. This agrees with the fact that the electric fields around *Rp. viridis* PRU/LM are sufficiently screened at the salt concentrations employed. Moreover, *Rp. viridis* RC/LM in Tris buffer (pH 8.0) exhibited neither large values nor large fluctuations of A_{ppt} and B_{ppt} (Fig. 6A, B, D, and E). This indicates that the large values and fluctuations of the two parameters of *Rp. viridis* PRU/LM are attributed to the presence of LH1-subunit surrounding the RC.

Due to the presence of LH1-subunit, *Rp. viridis* PRU particles are difficult to be in close contact with themselves and PEG molecules. It follows that there are relatively large particle−particle and particle−PEG interspaces that accommodate solvent molecules such as water and ions. Moreover, each protomer in the LH1-subunit possesses many ionizable and polar residues [47] on the extra-micellar surfaces in addition to the partial charges [8] at both structural ends of the 32 α-helices. Hence, the extra-micellar surfaces can attract many water molecules and ions. The solvent molecules not only prevent the particle−particle contact but also facilitate ejection of PEG molecules from interparticle spaces. This seems to be reflected as the large values of A_{ppt} and B_{ppt}. Moreover, the solvent molecules are not immobilized on the extra-micellar surfaces but with some freedom in configuration and direction. This should be one of the causes for the large fluctuations in the variations of A_{ppt} and B_{ppt}.

It is unlikely that the strength of electric field from the α-helices differs to a considerable extent between the LH1-subunit of *Rp. viridis* PRU and the two kinds of LH2s. However, *Rp. viridis* PRU/LM did not exhibit local maxima of A_{ppt} and B_{ppt} for SO_4^- and HPO_4^{2-}. As explained in the preceding paragraph, *Rp. viridis* PRU intrinsically exhibits large values and fluctuations of A_{ppt} and B_{ppt} for various ionic species. Since short-range steric repulsion thus sufficiently contributes to the particle−particle and particle−PEG interactions, the two parameters are difficult to exhibit larger values for the two anionic species. Besides, electric fields from charges and dipoles of H- [39] and cytochrome-subunits [41], pointing to various directions, act on the solvent molecules in an additional manner to the electric field from the LH1-subunit. The resultant electric fields around both ends of LH1-subunit are partially weakened, resulting in a decrease in number of ions that can strongly interact with the extra-micellar surfaces of LH1-subunit. This may be another reason for the A_{ppt} and B_{ppt} not exhibiting local maxima for the two anionic species.

In contrast to the result in the presence of monovalent cations, the A_{ppt} of *Rp. viridis* PRU/LM did not exhibit conspicuously large values in the presence of divalent cations, compared with that of the other four kinds of proteins (Fig. 6A). In addition, the amorphous precipitates formed in the presence of divalent cations were more rigid

https://doi.org/10.1016/j.heliyon.2018.e01073

than those formed in the presence of monovalent ones. These results imply that the interparticle interaction is contributed to not only by short-range steric repulsion based on the presence of ions but also by effects of divalent cations such as ion-correlation force [27, 28, 29] and ionic bridging that can generate relatively strong attractive effects between the adjacent particles even at the low salt concentrations [8].

The values of $[P]_5$ of *Rp. viridis* PRU/LM were smaller than those of the other four kinds of protein/LM particles (Fig. 6C and F). This reflects that the large values of B_{ppt} have a stronger effect than the large values of A_{ppt} in determining the values of $[P]_5$. Due to the small values of $[P]_5$, *Rp. viridis* PRU/LM exhibits a rather good linear relationship between $[P]_5$ and $S_{\pm}$. Thus, even for *Rp. viridis* PRU that differs from the other proteins regarding the dependence of A_{ppt} and B_{ppt} on ionic species, the linear relationship expressed by Eq. (2) is retained.

With of *Rp. viridis* PRU/LM, the values and variations of $[P]_5$ for $S_{\pm}$ were small, unlike those of A_{ppt} and B_{ppt}. This relationship is analogous to the following property of a right triangle with a base of a unit length and a variable elevation angle θ. In the triangle, the value of *tan* θ corresponds to the values of A_{ppt} and B_{ppt}. The variation of *tan* θ for the same increment $\Delta\theta$, that is, *tan* $(\theta + \Delta\theta)$ - *tan* θ, increases with θ, where $0 < \theta + \Delta\theta < \pi/2$. However, the value 5/*tan* $(\theta + \Delta\theta)$ - 5/*tan* θ, corresponding to the variation of $[P]_5$, gradually decreases to zero with increasing θ. Thus, when the slopes of PCs are steep, even small measurement errors included in the PCs are noticeably emphasized in the intercept A_{ppt} and slope B_{ppt}. This relationship also applies to the result of *Rb. sphaeroides* LH2/MEGA9 where the slope of the $[P]_5$ plots against $S_{\pm}$ is rather gentle in spite of the obviously large variations of A_{ppt} and B_{ppt}.

3.5.3. *Rp. viridis* and *Rb. sphaeroides* RCs

Rp. viridis RC is a hetero-tetramer of L-, M-, H- and cytochrome-subunits [42, 43], whereas *Rb. sphaeroides* RC is a hetero-trimer of L-, M- and H-subunits [48]. Due to this difference, the property of extramembranous regions is quite different between the two RCs. With *Rp. viridis* RC/LM and *Rb. sphaeroides* RC/LM in Tris buffer (pH 8.0), the A_{ppt} gradually increased and the B_{ppt} gradually decreased with $S_{\pm}$ (Fig. 6A, B, D and E); the two kinds of RCs did not exhibit such irregular values of the two parameters as the two kinds of LH2s exhibited. As a result of the gradual variations, the $[P]_5$ of the two kinds of RCs varied gradually with $S_{\pm}$; the values of $[P]_5$ were scattered to the same extent around the mean lines of $[P]_5$ plotted against $S_{\pm}$ as those of the other three kinds of proteins (Fig. 6C and F).

If neither adsorption of ions to particles nor state change of particles occurs, particle−particle and particle−PEG interactions do not conspicuously vary against

https://doi.org/10.1016/j.heliyon.2018.e01073

the change of ionic species along the increasing density and number of partial charges on the ionic surface, resulting in gradual variations of A_{ppt} and B_{ppt} with $S_{\pm}$. Such variations are exemplified by the two kinds of RCs that have neither a large cluster of similar charges nor a large cluster of hydrophobic residues on their extra-micellar surfaces [39, 40, 41, 42, 43, 48, 49]. Around such proteins, the rotational motion of ions is not strongly restricted, and therefore the ions can point to various directions. Thus, the values of $S_{\pm}$ appear to reflect the electrical interaction ability of ions whose anisotropic properties are angle-averaged to some extent. However, the relationship between the values of $S_{\pm}$ and the strength of interaction ability of ions is opposite in the cases of cations and anions (cf. Table2), because the solvent effects relevant to cations are not the same as those relevant to anions, as explained about Fig. 1.

The A_{ppt} of *Rb. sphaeroides* RC/LDAO (green symbols) discontinuously increased when cationic species was replaced from Mg^{2+} to Na^{+} (Fig. 6A), like the A_{ppt} of *Rb. sphaeroides* LH2/LDAO (red symbols). However, such variation was not observed with *Rb. sphaeroides* RC/LM. This means that the discontinuous increase of A_{ppt} of *Rb. sphaeroides* RC/LDAO reflects some changes in the state of LDAO cluster. The A_{ppt} of *Rb. sphaeroides* RC/LDAO increased with increasing S_{+} of divalent cations and was nearly constant for monovalent cations (Fig. 6A). This variation of A_{ppt} against S_{+} is analogous to that of *Rb. sphaeroides* LH2/LDAO, though the values themselves of A_{ppt} differ between the two kinds of LDAO particles. This analogy seems to reflect the same variation of LDAO cluster as explained about *Rb. sphaeroides* LH2/LDAO in Fig. 5.

For cations, the slope of A_{ppt} plotted against S_{+} of monovalent cations was gentler than that against S_{+} of divalent cations (Fig. 6A). On the other hand, the down slope of B_{ppt} plotted against S_{+} of monovalent cations was steeper than that against S_{+} of divalent cations (Fig. 6B). Thus, the lines A_{ppt}−S_{+} and B_{ppt}−S_{+} bent between divalent and monovalent cations, resulting in a relatively good linear relationship between $[P]_5$ and S_{+} *Rb. sphaeroides* RC/LDAO exhibited (Fig. 6C).

For anions, the A_{ppt} values of *Rb. sphaeroides* RC/LDAO were not particularly large as compared with those of the other particles (Fig. 6D). However, the B_{ppt} values of *Rb. sphaeroides* RC/LDAO were obviously smaller than those of the other particles (Fig. 6E). As a result, the $[P]_5$ values of *Rb. sphaeroides* RC/LDAO were larger than those of the other particles (Fig. 6F). Moreover, the two parameters of *Rb. sphaeroides* RC/LDAO exhibited smaller variations than those of the other particles. However, the $[P]_5$ of *Rb. sphaeroides* RC/LDAO fluctuated to a large extent. This is because the variation of A_{ppt} is emphasized due to the obviously small values of B_{ppt}. However, in the sense that the $[P]_5$ does not exhibit irregular values for specific ionic species, a linear relationship between $[P]_5$ and S_{-} can also be recognized in the case with *Rb. sphaeroides* RC/LDAO.

https://doi.org/10.1016/j.heliyon.2018.e01073

3.6. Linearity of variation of $[P]_5$ against $S_\pm$ depending on hydrophilicity and hydrophobicity of particles

The variations of A_{ppt} and B_{ppt} for ionic species were reasonably related to those of particle−particle and particle−PEG interactions, respectively, upon considering the behavior of ions around hydrophilic groups and hydrophobic groups. When electrostatic interaction ability of ions increases, solvent effects around hydrophilic groups and solvent effects around hydrophobic groups vary so as to cancel their opposing influence on the individual interactions. In addition, the linear relationship between $[P]_5$ and $S_\pm$ arises from the correlative variations of A_{ppt} and B_{ppt} for ionic species. If it is taken into consideration that any protein is constituted of amino acids with hydrophilic and hydrophobic residues, Eq. (2) appears to be applicable to other proteins.

Variations of hydrophilic 'repulsion' and hydrophobic 'attraction' for ionic species do not always cancel, to a moderate extent, their opposing effects on the particle−particle and particle−PEG interactions because of their non-additive property. This seems to be one of the reasons to decrease linearity of the relationship between $[P]_5$ and $S_\pm$. In the presence of PEG, highly hydrophilic particles such as *Rb. sphaeroides* LH2/MEGA9 and *Rp. viridis* PRU/LM are easy to be separated from solution phase due to a large number of solvent molecules interacting with the particles [8]. Since the $[P]_5$ values of hydrophilic particles are thus intrinsically small for various ionic species, the variations of $[P]_5$ are also small. By contrast, particles possessing many hydrophobic groups on the surface such as *Rb. sphaeroides* LH2/$C_{12}E_8$ are a little difficult to be separated from solution phase due to the particle−PEG hydrophobic 'attraction' [8]. Since the $[P]_5$ values of somewhat hydrophobic particles are thus intrinsically large for various ionic species, the variations of $[P]_5$ are also large. Thus, the linear relationship between $[P]_5$ and $S_\pm$ may be degraded with increasing hydrophobicity of particles. This tendency can be a measure to consider applicability of Eq. (2) to other proteins.

3.7. Reproducibility of dependence of PCs on ionic species

The PCs whose A_{ppt}, B_{ppt} and $[P]_5$ values are plotted in Figs. 5 and 6 were determined according to the following procedure. For three or four salt species, preliminary PCs were first determined from supernatant protein concentrations measured at PEG concentrations with 10 mg/mL intervals. By the application of Eq. (2) to the preliminary PCs, ranges of PEG concentration with which supernatant protein concentration would decrease were evaluated for the 22 salt species. In experiments planned on the basis of the evaluated ranges of PEG concentration, supernatant protein concentrations were measured at 12 or more PEG concentrations with 5 or 2.5 mg/mL intervals. For most salt species, the horizontal positions of PCs thus determined agreed with those predicted from the preliminary PCs. Besides, although

https://doi.org/10.1016/j.heliyon.2018.e01073

the molecular weighs of PEG employed were not 4000, *Rp. viridis* PRU/LM, *Rb. sphaeroides* LH2/LM and *Rb. capsulatus* LH2/LM exhibited the same dependence of PC on ionic species as observed in this study. This result will be shown in our separate study (in preparation). Thus, it was ascertained in the two ways that the dependence of PC on ionic species shown in Figs. 5 and 6 was reproducible.

3.8. Influences of change in solution pH on PC

Since addition of a salt changes pH of aqueous solution, the dissociation degree of ionizable groups changes depending on the salt species. To study influences of the pH change on particle−particle and particle−PEG interactions, the dependence of A_{ppt} and B_{ppt} on solution pH was investigated. With the five kinds of particles indicated in Fig. 6, the values of A_{ppt} and B_{ppt} are plotted against the pH in Fig. 7. In several cases, the A_{ppt} and B_{ppt} appear to vary linearly with pH at first sight. However, this linear relationship is fortuitous as described in the following paragraphs.

The pIs of *Rp viridis* PRU/LM (open circles) and *Rp viridis* RC/LM (open squares) were in the pH range of Tris buffer (7.0−8.9) to which various nitrates and potassium salts were separately added. However, the A_{ppt} values of the two kinds of particles did not exhibit such a trough at pH values near their pIs (Fig. 7A and C) as those of human and bovine albumins did [3]. Moreover, the pH ranges of Tris buffer for nitrates and potassium salts overlapped in the pH range of 7.6−8.4. When pH was raised in the overlapping range, the A_{ppt} of *Rp viridis* RC/LM and *Rb. sphaeroides* RC/LM (green symbols) increased for the nitrates but decreased for the potassium salts. Thus, in spite of the same variation in pH, the A_{ppt} varied to the opposite directions for the nitrates and the potassium salts. Moreover, in spite of the same variation in pH, the A_{ppt} of *Rb. sphaeroides* LH2/LM (red symbols) and *Rb. capsulatus* LH2/LM (blue symbols) exhibited a larger increase for the nitrates than for the potassium salts.

With *Rp viridis* RC/LM (closed squares) in BisTris buffer to which the salts were separately added, the A_{ppt} exhibited a slight increase for the nitrates (in the range of pH 3.8−6.3) and a slight decrease for the potassium salts (in the range of pH 6.1−8.0). Moreover, in both solutions of BisTris buffer and Tris buffer, *Rp viridis* RC/LM did not exhibit a trough at pH values near its pI in the variation of A_{ppt} with pH. These results are also opposite to the relationship observed with the result of albumins [3]. Thus, in most cases, the variation of A_{ppt} with pH is not correlated with the deviation of solution pH from the particle pI.

Such a weak correlation is rather natural for the following facts. First, in a salt solution, the magnitude and range of electrostatic forces between neighboring particles are sufficiently weakened due to both the high relative dielectric constant of water and the electrostatic screening effect of an ion. Second, the particle−particle

https://doi.org/10.1016/j.heliyon.2018.e01073

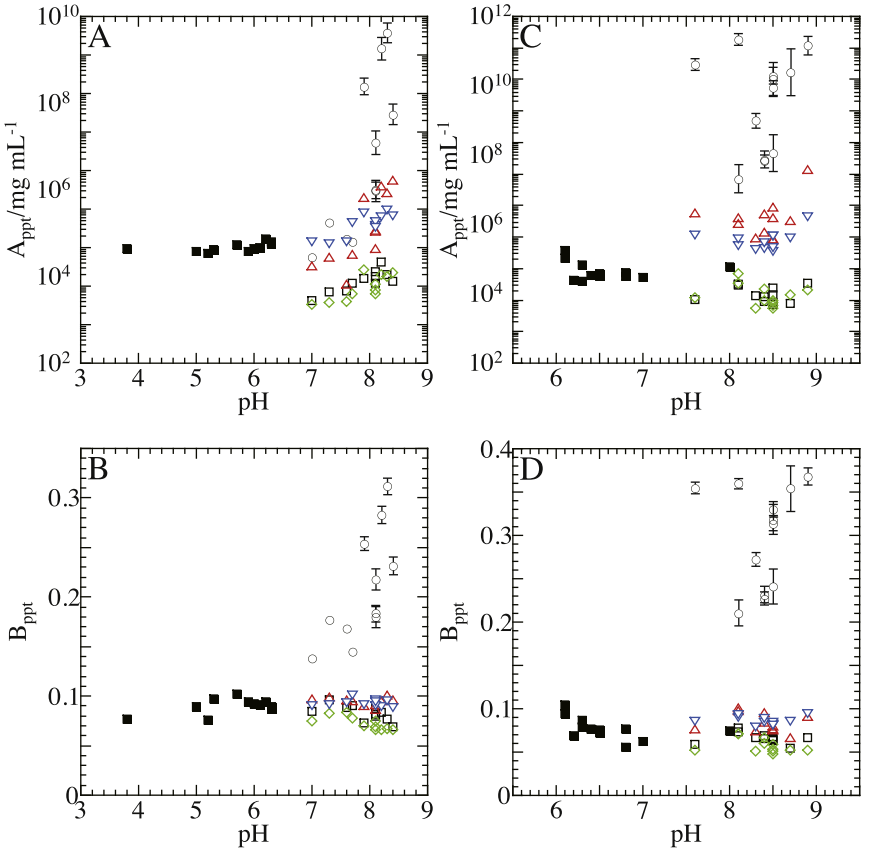

Fig. 7. Variations of intercept and slope of PC with solution pH observed with particles of different proteins. The values of (A and C) intercept A_{ppt} and (B and D) slope B_{ppt} are plotted against pH values of solution to which various salts are separately added. The protein/detergent particles and solution ingredients were as follows: *Rp. viridis* PRU/LM (◯), *Rp. viridis* RC/LM (□), *Rb. sphaeroides* RC/LM (◇), *Rb. sphaeroides* LH2/LM (△) and *Rb. capsulatus* LH2/LM (▽) in a Tris buffer solution (25 mM Tris−HCl, and 0.2 mg/mL NaN_3; pH 8.0), and *Rp. viridis* RC/LM (■) in a BisTris buffer solution (25 mM BisTris−HCl, and 0.2 mg/mL NaN_3; pH 6.0). The concentrations of LDAO and LM were 1 mg/mL. The error bars attached to symbols represent standard errors calculated by the least-square fitting; no error bar is shown for the standard errors that are similar to or smaller than the size of symbols.

interaction reflected by the values of A_{ppt} is not based on the center−to−center force but on the mean of forces between different parts on one particle and different parts on the other particle [8]. Moreover, the dissociation degree of ionizable residues is not much changed by the variation of pH in the range of $>$ 1.0 pH unit away from their dissociation constants.

With respect to the five kinds of particles, close correlation was not recognized between the value of B_{ppt} and the deviation of solution pH from the particle pI, either (Fig. 7B and D). This is attributable to the same reasons as mentioned in the preceding paragraph. Moreover, the dependence of B_{ppt} on pH was not the same as that of A_{ppt}, due to the difference in ratio of short-range steric repulsion to hydrophobic 'attraction' between the particle−particle and particle−PEG interactions. Thus, it

https://doi.org/10.1016/j.heliyon.2018.e01073

is understood that the association of particles solubilized by LM is influenced by the direct action of ions on the particles and solvent rather than the change in pH (the indirect effect of ions).

3.9. PC of *Rb. sphaeroides* LH2/OG for a mixture of $NaNO_3$ and $Mg(NO_3)_2$

Mixtures of two or more salt species are frequently employed as precipitants in combination with PEG—for instance, to improve crystallizability and crystal quality of macromolecules. To study effects of salt mixtures on macromolecular association, PCs were determined for *Rb. sphaeroides* LH2/OG at various concentrations of $NaNO_3$/$Mg(NO_3)_2$ mixture. Most of the PCs determined followed Eq. (1). If the added salts contained adsorptive ionic species, particles or PEG molecules with different properties should coexist at such low concentrations of the salt mixture at which all adsorptive sites on the surfaces of particles or PEG molecules are not bound with the ions. In such solutions, the concentration of particles remaining in the solution phase cannot decrease in a single exponential manner with increasing PEG concentration. Thus, it is seen that ions dissociated from the mixture are not strongly adsorbed to the particles and PEG molecules.

The values of A_{ppt}, B_{ppt} and $[P]_5$ evaluated from the PCs determined are plotted against the 'effective concentrations' of $NaNO_3$ and $Mg(NO_3)_2$ in a contour presentation in Fig. 8. When the concentration of the salt mixture was increased, the values of A_{ppt}, B_{ppt} and $[P]_5$ decreased at a declining rate. Such a variation in the three parameters was also observed in the case where the eighteen species of salts were separately added [8], except for phosphate salts whose addition caused the sample solution into two immiscible (salt- and PEG-rich) aqueous phases at 0.15 M or higher [8, 18]. The variations of the three parameters are related to that there is neither strong ion−ion interference nor adsorption of ions to the particles or PEG molecules, because of the following reasons. First, it is hardly conceivable that all salts employed contained adsorptive ionic species. Second, if the dissociated ions were adsorbed to the particles or PEG molecules, the reduction of ionic concentration in the solution phase should be reflected as peculiar variations of A_{ppt} and B_{ppt} at low salt concentrations. Moreover, if insoluble salts were formed, the electrostatic screening effect would be weakened by the amount of salt that was separated as insoluble materials from the solution phase. However, such influences were not observed. In fact, the salt mixture did not contain any pair of ionic species to form a salt that was known to be insoluble in water.

When the sum of 'effective concentrations' of $Mg(NO_3)_2$ and $NaNO_3$ was 0.4 or higher, the A_{ppt}, B_{ppt} and $[P]_5$ decreased linearly with 'effective concentration'. This result implies that in the range of 'effective concentrations', the electric fields around *Rb. sphaeroides* LH2/OG are sufficiently screened, as explained in our

https://doi.org/10.1016/j.heliyon.2018.e01073

preceding study [8]. Moreover, when the composition of salt mixture was varied from $Mg(NO_3)_2$ to $NaNO_3$ while the total 'effective concentration' being maintained at a constant value [k_{eff}], the values of A_{ppt}, B_{ppt} and $[P]_5$ varied from their values for $Mg(NO_3)_2$ of [k_{eff}] to ones for $NaNO_3$ of [k_{eff}] in an approximately linear manner. Such variation is expressed by the following equation:

$$\begin{aligned} Q(M\left[m_{eff}\right] + N\left[n_{eff}\right]) = \{ & m_{eff} \cdot Q(M\left[m_{eff} + n_{eff}\right]) \\ & + n_{eff} \cdot Q(N\left[m_{eff} + n_{eff}\right]\}/(m_{eff} + n_{eff}), \end{aligned} \tag{3}$$

where Q(M [m_{eff}] + N [n_{eff}]) is values of A_{ppt}, B_{ppt} or $[P]_5$ for the salt mixture containing $Mg(NO_3)_2$ of [m_{eff}] and $NaNO_3$ of [n_{eff}], Q(M [m_{eff} + n_{eff}]) for $Mg(NO_3)_2$ of [m_{eff} + n_{eff}], Q(N [m_{eff} + n_{eff}]) for $NaNO_3$ of [m_{eff} + n_{eff}], and [m_{eff} + n_{eff}] = [k_{eff}] is constant.

This equation shows that the fraction of 'effective concentration' determines the ratio of the effect of each constituent salt in the total effect of the salt mixture on the particle−particle and particle−PEG interactions. This was also observed in other cases. For instance, the values of A_{ppt}, B_{ppt} and $[P]_5$ of the fifteen kinds of particles for potassium sodium tartrate of 0.4 in terms of the 'effective concentration' unit exhibited means of the corresponding values for potassium tartrate and sodium tartrate of the same 'effective concentration'. These results suggest that the relationship expressed by Eq. (3) will be applicable to other kinds of particles, unless a salt mixture contains ions that strongly interact with the particles, PEG molecules or their counter ions. Thus, the 'effective concentration' provides a useful measure to express the effect of the salt mixture on the particle association.

3.10. Application to initial crystallization screening of *Rs. Rubrum* PRU

The primary concern of this study is to advance understanding of roles and effectiveness of salts in macromolecular association. Nevertheless, the relationships deduced in this study can be applied to other purposes—for instance, initial screening of macromolecular crystallization for which adequate PEG concentrations are evaluated by referring to the PCs of macromolecules [6, 9]. Prior to the screening experiment, we chose 0.4 in terms of 'effective' concentration unit as salt concentrations to employ. This was due to the observation that unless salt−PEG phase separation occurred in sample solutions [9, 20], protein/detergent particles were easily crystallized at such relatively high salt concentrations as for the interparticle electrostatic forces to be sufficiently screened. The reason for this correlation between the crystallizability and the electrostatic state of particles will be explained in our separate study (in preparation).

As an example, initial crystallization screening of *Rs. Rubrum* PRU solubilized by *N*−decyl−β−*D*−maltopyranoside (DM) by a vapor diffusion method was planned

https://doi.org/10.1016/j.heliyon.2018.e01073

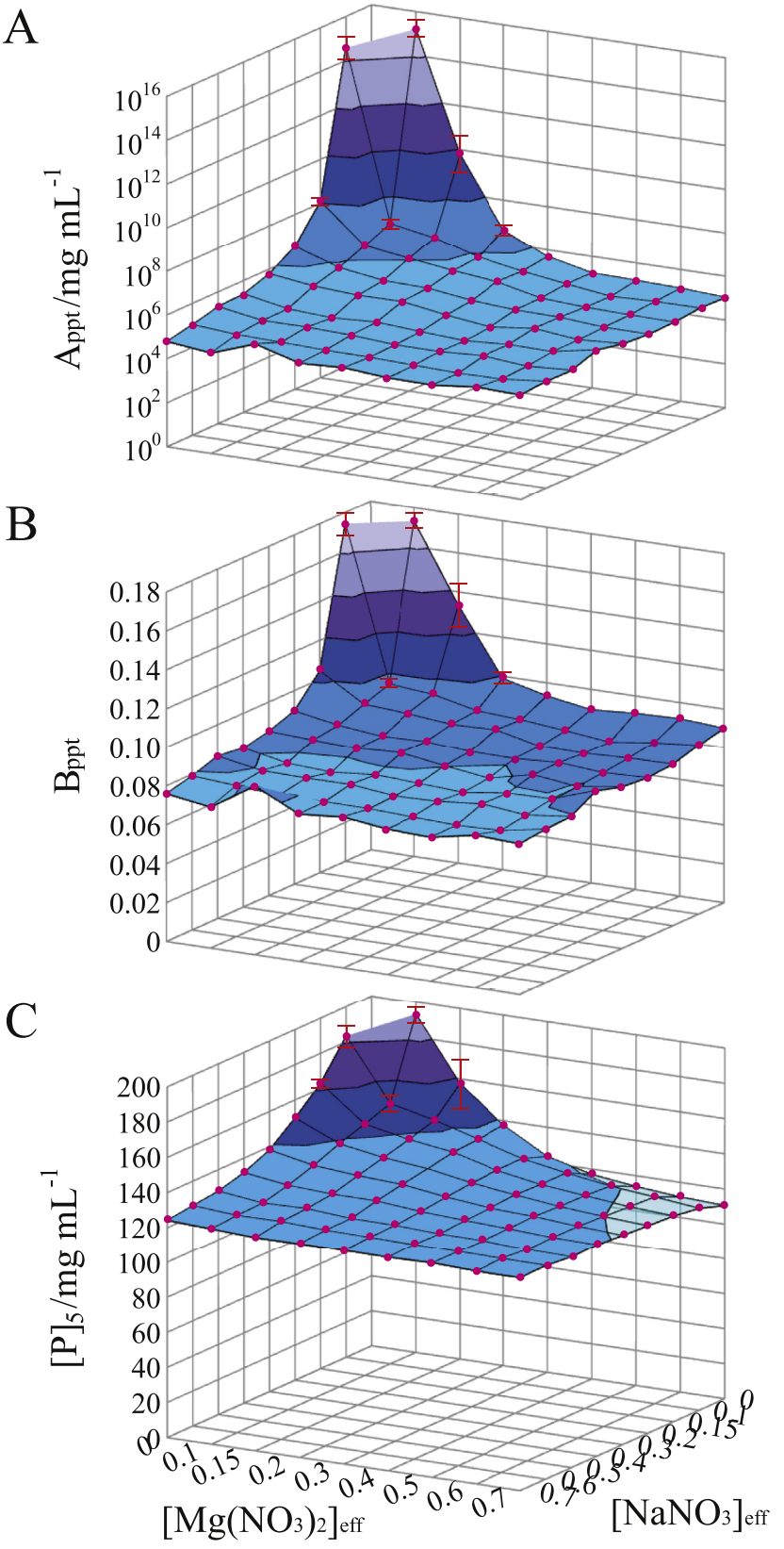

https://doi.org/10.1016/j.heliyon.2018.e01073

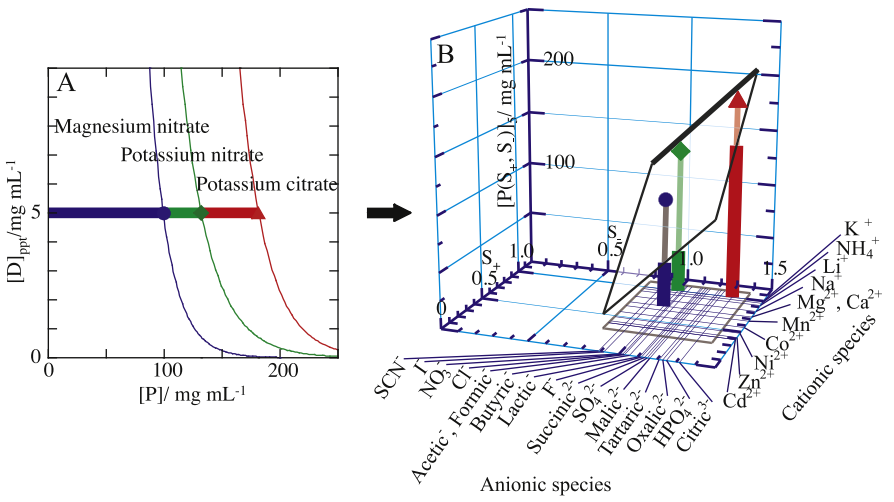

Fig. 9. Schematic representation of the relationship between horizontal position of PC and ionic species dissociated from salts added. A; PCs of a target protein/detergent particle experimentally obtained for three salt species at the same 'effective concentration'—0.4 M potassium nitrate, 0.133 M potassium citrate, and 0.04 M magnesium nitrate, for example. For electric field around the particle to be sufficiently screened without salt−PEG phase separation, the concentrations of individual salts to add are empirically 0.3 to 0.4 in terms of 'effective salt concentration'. B; the three parameters F, G and H in Eq. (2) are evaluated by using the $[P]_5$ values (PEG concentration at which the protein concentration $[D]_{ppt}$ in supernatant is 5 mg/mL) of the three PCs experimentally obtained and the $S_{\pm}$ values (shown in Table 1) of ionic species that constitute the three salt species added. By substituting the evaluated values of the three parameters and the $S_{\pm}$ values of ionic species that constitute a desired salt species into Eq. (2), the value of $[P]_5$ is calculated for the desired salt. Likewise, the values of $[P]_{20}$ and $[P]_1$ were evaluated for the sample and reservoir solutions in the initial crystallization screening of *Rs. Rubrum* PRU/DM, respectively.

and performed in the following procedure. Here, it is noted that the primary structure and thermal stability are different between *Rs. Rubrum* PRU and *Rp. viridis* PRU due to their difference in constituent subunits [50]. PCs in the presence of 20 mg/mL protein were determined for KNO_3, $Mg(NO_3)_2$ and tri−potassium citrate, though the accuracy of the PCs was as low as that of preliminary PCs mentioned above. By the application of Eq. (2) to the three PCs determined, for other 72 salt species, PEG concentrations at which concentrations of protein dispersed in sample solutions would be 20 mg/mL and 1 mg/mL were evaluated for sample and reservoir solutions, respectively (cf. Fig. 9). By the use of Eq. (3), PEG concentration for potassium sodium tartrate was further calculated from the two PEG concentrations evaluated for

Fig. 8. PC of *Rb. sphaeroides* LH2/OG for mixtures of $NaNO_3$ and $Mg(NO_3)_2$ of various 'effective concentrations'. The values of (A) intercept A_{ppt}, (B) slope B_{ppt} and (C) horizontal position $[P]_5$ were based on the best-fitted PCs. The coordinates of red circles against the 'effective concentrations' represent the experimental values of the three parameters. The other solution ingredients were 25 mM Tris−HCl (pH 8.0) and 0.2 mg/mL NaN_3, and 8 mg/mL OG. The error bars attached to the red circles represent standard errors calculated by the least-square fitting; no error bar is shown for the standard errors that are similar to or smaller than the size of red circles.

https://doi.org/10.1016/j.heliyon.2018.e01073

Table 3. PEG concentrations forecasted for 20 (left side) and 1 mg/mL (right side) of *Rs. rubrum* PRU/DM in supernatant.

	Li^+	Na^+	K^+	NH_4^+	Mg^{2+}	Ca^{2+}	Mn^{2+}	Co^{2+}	Ni^{2+}	Zn^{2+}	Cd^{2+}
F^-		64–93*	65–93	65–93*							
Cl^-	64–91	63–91*	64–91*	64–91*	62–92	62–92	62–92	61–92	60–92	60–92*	60–92
I^-		62–90*	63–90*	63–90*							
NO_3^-	63–91*	63–91*	64–91*	64–91*	62–91	62–91*	61–91	61–92	60–92	60–92*	59–92
SCN^-		61–90*	62–89*	62–89*							
$Formic^-$		63–92*	64–91*	64–91*	62–92	62–92*	62–92			60–92*	60–92
$Acetic^-$	64–91	63–92*	64–91*	64–91*	62–92	62–92	62–92	61–92	60–92	60–92	60–92
$Lactic^-$	65–93										
$Butyric^-$		63–92*									
SO_4^{2-}	65–93*	64–93	66–93	66–93*	64–93		63–94	63–94	62–94	61–94*	61–94
$Tartric^{2-}$		65–94*	66–94								
$Malic^{2-}$		65–93*									
$Succinic^{2-}$		64–93*									
$Oxalic^{2-}$	66–94*		67–94*								
HPO_4^{2-}		66–95	67–94	67–94							
$Citric^{3-}$	67–96*	67–96	68–95*	68–95*					Na,K-tartrate: 66–94*		

*Crystals were formed.

https://doi.org/10.1016/j.heliyon.2018.e01073

di−potassium tartrate and di−sodium tartrate. For phosphate-containing salts, the PEG concentrations for sample and reservoir solutions might be lower and higher than the true concentrations at which the supernatant protein concentrations would be 20 and 1 mg/mL, respectively, as demonstrated in Fig. 1. However, no corrections were made for the forecasted deviations, because of the comparatively slow evaporation of water from a PEG-containing aqueous solution [51]. Thus, PEG concentrations to prepare in sample and reservoir solutions were evaluated so that the composition of sample solutions could proceed in a crystallizable zone with time [8]. The PEG concentrations evaluated are shown in Table 3.

PEG concentrations of sample and reservoir solutions were prepared to be the values shown in Table 3. Most of the prepared sample solutions were slightly turbid, which meant that the prepared PEG concentrations were adequate for the starting sample solutions [9]. The amorphous precipitates formed were removed by centrifugation so as not to undesirably influence the crystallization. The sample solutions placed in separate air-tight containers for individual salts were incubated at 20 °C, in darkness, for one week. *Rs. rubrum* PRU/DM was crystalized for 39 salt species of 76 ones examined, as also indicated in Table 3. Besides, in other screening experiments performed likewise, *Rp. viridis* PRU/DM and *Rb. sphaeroides* RC/OG were also crystallized at high ratios. These results suggest that Eqs. (2) and (3) will be usable for rationalizing crystallization screening in cooperation with high-throughput technologies [7].

4. Conclusions

Salt/polyethylene glycol (PEG) mixtures are precipitants for biological macromolecules. The dependence of precipitation curves (PCs) on salt species was investigated for integral membrane protein/detergent particles to reveal the following roles and effects of various ions. In the presence of ions whose interaction with water is stronger than water−water interaction, coordination of solvent molecules is rearranged to strengthen short-range steric repulsion and hydrophobic attraction. In the presence of ions whose interaction with water is weaker than water−water interaction, hydrophobic−hydrophobic contacts are hindered. Moreover, strong electric fields of divalent cations cause attractive effects between electronegative or polar groups of neighboring particles. The particle−particle and particle−PEG interactions, determined by these solvent effects, vary in a correlative manner with strengthening electrostatic interaction ability of ions even in the cases of comparatively strong ion−particle interaction. Accordingly, the relationship between horizontal positions of PC and salt species in the pH range of 5.0−9.0 can be formulated as a binary linear function of the interaction ability of cations and anions. The binary linear function is also usable in the case of employing a salt mixture by using the fraction of 'effective concentration' of constituent salts as a weight factor.

https://doi.org/10.1016/j.heliyon.2018.e01073

Declarations

Author contribution statement

Takayuki Odahara: Conceived and designed the experiments; Performed the experiments; Analyzed and interpreted the data; Wrote the paper.

Koji Odahara: Performed the experiments; Analyzed and interpreted the data.

Funding statement

This research did not receive any specific grant from funding agencies in the public, commercial, or not-for-profit sectors.

Competing interest statement

The authors declare no conflict of interest.

Additional information

No additional information is available for this paper.

Acknowledgements

We are grateful to Dr. N. Ishii of AIST for his constructive criticism on the manuscript.

References

[1] I.R.M. Juckes, Fraction of proteins and viruses with polyethylene glycol, Biochim. Biophys. Acta 229 (1971) 535−546.

[2] A. McPherson, The growth and preliminary investigation of protein and nucleic acid crystals for X-ray diffraction analysis, Methods Biochem. Anal. 23 (1976) 249−345.

[3] K.C. Ingham, Precipitation of proteins with polyethylene glycol: characterization of albumin, Arch. Biochem. Biophys. 186 (1978) 106−113.

[4] T. Arakawa, S.N. Timasheff, Theory of protein solubility, Methods Enzymol. 114 (1985) 49−77.

[5] W. Kühlbrandt, Three−dimensional crystallization of membrane proteins, Q. Rev. Biophys. 21 (1988) 429−477.

https://doi.org/10.1016/j.heliyon.2018.e01073

[6] T. Odahara, M. Ataka, T. Katsura, Phase diagram determination to elucidate the crystal growth of the photoreaction center from *Rhodobacter sphaeroides*, Acta Cryst. D50 (1994) 639−642.

[7] L. Yibin, What's happened over the last five years with high-throughput protein crystallization screening? Expert Opin. Drug Discov. 13 (2018) 691−6695.

[8] T. Odahara, K. Odahara, Intermolecular interactions at early stage of protein/detergent particle association induced by salt/polyethylene glycol mixtures, Protein Expr. Purif. 120 (2016) 72−86.

[9] T. Odahara, Stability and solubility of integral membrane proteins from photosynthetic bacteria solubilized in different detergents, Biochim. Biophys. Acta 1660 (2004) 80−92.

[10] A.A. Green, Studies in the physical chemistry of the proteins X. The solubility of hemoglobin in solutions of chlorides and sulfates of varying concentration, J. Biol. Chem. 95 (1932) 47−66. http://www.jbc.org/content/95/1/47.full.pdf.

[11] S.N. Timasheff, T. Arakawa, Mechanism of protein precipitation and stabilization by co-solvents, J. Cryst. Growth 90 (1988) 39−46.

[12] R.K. Clayton, B.J. Clayton, Molar extinction coefficients and other properties of an improved reaction center preparation from *Rhodopseudomonas viridis*, Biochim. Biophys. Acta 501 (1978) 478−487.

[13] R.J. Cogdell, J.G. Lindsay, G.P. Reid, G.D. Webster, A comparison of the constituent polypeptides of the B−[800]−850 light−harvesting pigment-protein complex from *Rhodopseudomonas sphaeroides*, Biochim. Biophys. Acta 591 (1980) 312−320.

[14] H.A. Frank, S.S. Taremi, J.R. Knox, Crystallisation and preliminary X-ray and optical spectroscopic characterisation of the photochemical reaction center from *Rhodobacter sphaeroides* strain 2.4.1, J. Mol. Biol. 198 (1987) 139−141.

[15] M. Hara, K. Namba, Y. Hirata, T. Majima, S. Kawamura, Y. Asada, J. Miyake, The photoreaction unit in *Rhodopseudomonas viridis*, Plant Cell Physiol. 31 (1990) 951−960.

[16] W. Welte, T. Wacker, Protein−detergent micellar solutions for the crystallization of membrane proteins: some general approaches and experiences with the crystallization of pigment−protein complexes from purple bacteria, in: H. Michel (Ed.), Crystallization of Membrane Proteins, CRC Press, Boca Raton, FL, 1991, pp. 107−123.

https://doi.org/10.1016/j.heliyon.2018.e01073

[17] R.J. Cogdell, K.J. Woolley, L.A. Ferguson, D.J. Dawkins, Crystallisation of purple bacterial antenna complexes, in: H. Michel (Ed.), Crystallization of Membrane Proteins, CRC Press, Boca Raton, FL, 1991, pp. 125−136.

[18] T. Odahara, K. Odahara, Data in support of intermolecular interactions at early stage of protein/detergent particle association induced by salt/polyethylene glycol mixtures, Data Brief 7 (2016) 1283−1287.

[19] F.E. Bailey, R.W. Callard, Some properties of poly(ethylene oxide) in aqueous solution, J. Appl. Polym. Sci. 1 (1959) 56−62.

[20] J.C. Lee, L.L.Y. Lee, Preferential solvent interactions between proteins and polyethylene glycols, J. Biol. Chem. 256 (1981) 625−631. http://www.jbc.org/content/256/2/625.full.pdf.

[21] S.A. Oelmeier, F. Dismer, J. Hubbuch, Molecular dynamics simulations on aqueous two−phase systems − single PEG−molecules in solution, BMC Biophys. 5 (2012).

[22] C. Horváth, W. Melander, I. Molnár, Solvophobic interactions in liquid chromatography with nonpolar stationary phases, J. Chromatogr. 125 (1976) 129−156.

[23] L.M.P. Beekman, R.N. Frese, G.J.S. Fowler, R. Picorel, R.J. Cogdell, I.H.M. van Stokkum, C.N. Hunter, R. van Grondelle, Characterization of the light−harvesting antennas of photosynthetic purple bacteria by Stark spectroscopy. 2. LH2 complexes: influence of the protein environment, J. Phys. Chem. B 101 (1997) 7293−7301.

[24] D.E. Chandler, J. Hsin, C.B. Harrison, J. Gumbart, K. Schulten, Intrinsic curvature properties of photosynthetic proteins, Biophys. J. 95 (2008) 2822−2836.

[25] J.N. Israelachvili, Interactions involving polar molecules, in: Intermolecular and Surface Forces, second ed., Academic Press, 1992, pp. 48−66.

[26] A. George, Y. Chiang, B. Guo, A. Arabshahi, Z. Gai, W.W. Wilson, Second virial coefficient as predictor in protein crystal growth, Methods Enzymol. 276 (1997) 100−110.

[27] L. Guldbrand, B. Jönsson, H. Wennerström, P. Linse, Electrical double layer forces. a Monte Carlo study, J. Chem. Phys. 80 (1984) 2221−2228.

[28] J. Marra, Direct measurements of attractive van der Waals and adhesion forces between uncharged lipid bilayers in aqueous solutions, J. Colloid Interface Sci. 109 (1986) 11−20.

https://doi.org/10.1016/j.heliyon.2018.e01073

[29] J. Marra, Effects of counterions specificity on the interactions between quaternary ammonium surfactants in monolayers and bilayers, J. Phys. Chem. 90 (1986) 2145−2150.

[30] S. Puvvada, D. Blanckstein, Molecular−thermodynamic approach to predict micellization, phase behavior and phase separation of micellar solutions. I. application to nonionic surfactants, J. Chem. Phys. 92 (1990) 3710−3724.

[31] S. Asakura, F. Oosawa, On interaction between two bodies immersed in a solution of macromolecules, J. Chem. Phys. 22 (1954) 1255−1256.

[32] S. Asakura, F. Oosawa, Interactions between particles suspended in solutions of macromolecules, J. Polym. Sci. [B] 33 (1958) 183−192.

[33] D.H. Atha, K.C. Ingham, Mechanism of precipitation of proteins by polyethylene glycols, J. Biol. Chem. 256 (1981) 12108−12117. http://www.jbc.org/content/256/23/12108.full.pdf.

[34] A. Pan, S.S. Mati, B. Naskar, S.B. Bhattacharya, S.P. Moulik, Self−aggregation of MEGA−9 (*N*−Nonanoyl−*N*−methyl−*D*−glucamine) in aqueous medium: physicochemistry of interfacial and solution behaviors with special reference to formation energetics and micelle microenvironment, J. Phys. Chem. B 117 (2013) 7578−7592.

[35] W. DeGrip, Thermal stability of rhodopsin and opsin in some novel detergents, Methods Enzymol. 81 (1982) 256−265.

[36] T. Walz, S.J. Jamieson, C.M. Bowers, P.A. Bullough, C.N. Hunter, Projection structures of three photosynthetic complexes from *Rhodobacter sphaeroides*: LH2 at 6 Å, LH1 and RC−LH1 at 25 Å, J. Mol. Biol. 282 (1998) 833−845.

[37] S. Scheuring, J. Seguin, S. Marco, D. Lévy, C. Breyton, B. Robert, J.−L. Rigaud, AFM characterization of tilt and intrinsic flexibility of *Rhodobacter sphaeroides* light harvesting complex 2 (LH2), J. Mol. Biol. 325 (2003) 569−580.

[38] N.H. Tadros, R. Frank, G. Drews, Localization of the exposed N−terminal region of the B800−[850]α and β light−harvesting polypeptides on the cytoplasmic surface of *Rhodopseudomonas capsulata* chromatophores, J. Bacteriol. 167 (1986) 96−100.

[39] H. Michel, K.A. Weyer, H. Gruenberg, F. Lottspeich, The 'heavy' subunit of the photosynthetic reaction center from *Rhodospeudomonas viridis*: isolation of the gene, nucleotide and amino acid sequence, EMBO J. 4 (1985) 1667−1672.

https://doi.org/10.1016/j.heliyon.2018.e01073

[40] H. Michel, K.A. Weyer, H. Gruenberg, I. Dunger, D. Oesterhelt, F. Lottspeich, The 'light' and 'medium' subunits of the photosynthetic reaction center from *Rhodopseudomonas viridis*: isolation of the genes, nucleotide and amino acid sequence, EMBO J. 5 (1986) 1149−1158.

[41] K.A. Weyer, F. Lottspeich, H. Gruenberg, F. Lang, D. Oesterhelt, H. Michel, Amino acid sequence of the cytochrome subunit of the photosynthetic reaction centre from the purple bacterium *Rhodopseudomonas viridis*, EMBO J. 6 (1987) 2197−2202.

[42] J. Deisenhofer, O. Epp, K. Miki, R. Huber, H. Michel, X−ray structure analysis of a membrane protein complex: electron density map at 3 Å resolution and a model of the chromophores of the photosynthetic reaction center from *Rhodopseudomonas viridis*, J. Mol. Biol. 180 (1984) 385−398.

[43] J. Deisenhofer, O. Epp, K. Miki, R. Huber, H. Michel, Structure of the protein subunits in the photosynthetic reaction centre of *Rhodopseudomonas viridis* at 3Å resolution, Nature 318 (1985) 618−624.

[44] I. Ikeda−Yamasaki, T. Odahara, K. Mitsuoka, Y. Fujiyoshi, K. Murata, Projection map of the reaction center−light harvesting 1 complex from *Rhodopsedomonas viridis* at 10Å resolution, FEBS Letters 425 (1998) 505−508.

[45] S. Scheuring, J. Seguin, S. Marco, D. Lévy, B. Robert, J.−L. Rigaud, Nanodissection and high−resolution imaging of the *Rhodopseudomonas viridis* photosynthetic core complex in native membranes by AFM, Proc. Natl. Acad. Sci. 100 (2003) 1690−1693.

[46] S. Saijo, T. Sato, T. Kumasaka, N. Tanaka, K. Harata, T. Odahara, Crystallization and preliminary X−ray studies on the reaction center−light-harvesting 1 core complex from *Rhodopseudomonas viridis*, Acta Cryst. F61 (2005) 83−86.

[47] R.A. Brunisholz, F. Jay, F. Suter, H. Zuber, The light-harvesting polypeptides of *Rhodopseudomonas viridis*: the complete amino-acid sequences of B1015−α, B1015−β and B1015−γ, Biol. Chem. Hoppe-Seyler 366 (1985) 87−98.

[48] J.P. Allen, G. Feher, T.O. Yeates, H. Komiya, D.C. Ress, Structure of the reaction center from *Rhodobacter sphaeroides* R−26: the protein subunits, Proc. Natl. Acad. Sci. U.S.A. 84 (1987) 6162−6166.

[49] J.C. Williams, L.A. Steiner, G. Feher, Primary structure of the reaction center from *Rhodopseudomonas sphaeroides*, Proteins 1 (1986) 321−325.

 https://doi.org/10.1016/j.heliyon.2018.e01073

[50] T. Odahara, N. Ishii, A. Ooishi, S. Honda, H. Uedaira, M. Hara, J. Miyake, Thermostability of *Rhodopseudomonas viridis* and *Rhodospirillum rubrum* chromatophores reflecting physiological conditions, Biochim. Biophys. Acta 1808 (2011) 1645−1653.

[51] V. Mikol, J.−L. Rodeau, R. Giegé, Changes of pH during biomacromolecule crystallization by vapor diffusion using ammonium sulfate as the precipitant, J. Appl. Crystallogr. 22 (1989) 155−161.

https://doi.org/10.1016/j.heliyon.2018.e01073